A Section 508–conformant HTML version of this article is available at https://doi.org/10.1289/EHP6336.

Uterine Patterning, Endometrial Gland Development, and Implantation Failure in Mice Exposed Neonatally to Genistein

Wendy N. Jefferson,[1] Elizabeth Padilla-Banks,[1] Alisa A. Suen,[1] Lindsey J. Royer,[2] Sharon M. Zeldin,[1] Ripla Arora,[2] and Carmen J. Williams[1]

[1]Reproductive and Developmental Biology Laboratory, National Institute of Environmental Health Sciences, National Institutes of Health, Department of Health and Human Services, Research Triangle Park, North Carolina, USA
[2]Department of Obstetrics, Gynecology, and Reproductive Biology, Institute for Quantitative Health Science and Engineering, College of Human Medicine, Michigan State University, East Lansing, Michigan, USA

Background: Embryo implantation relies on precise hormonal regulation, associated gene expression changes, and appropriate female reproductive tract tissue architecture. Female mice exposed neonatally to the phytoestrogen genistein (GEN) at doses similar to those in infants consuming soy-based infant formulas are infertile due in part to uterine implantation defects.

Objectives: Our goal was to determine the mechanisms by which neonatal GEN exposure causes implantation defects.

Methods: Female mice were exposed to GEN on postnatal days (PND)1–5 and uterine tissues collected on PND5, PND22–26, and during pregnancy. Analysis of tissue weights, morphology, and gene expression was performed using standard histology, confocal imaging with three-dimensional analysis, real-time reverse transcription polymerase chain reaction (real-time RT-PCR), and microarrays. The response of ovariectomized adults to 17β-estradiol (E2) and artificial decidualization were measured. Leukemia inhibitory factor (LIF) injections were given intraperitoneally and implantation sites visualized. Gene expression patterns were compared with curated data sets to identify upstream regulators.

Results: GEN-exposed mice exhibited reduced uterine weight gain in response to E2 treatment or artificial decidualization compared with controls; however, expression of select hormone responsive genes remained similar between the two groups. Uteri from pregnant GEN-exposed mice were posteriorized and had reduced glandular epithelium. Implantation failure was not rescued by LIF administration. Microarray analysis of GEN-exposed uteri during early pregnancy revealed significant overlap with several conditional uterine knockout mouse models, including *Foxa2*, *Wnt4*, and *Sox17*. These models exhibit reduced endometrial glands, features of posteriorization and implantation failure. Expression of *Foxa2*, *Wnt4*, and *Sox17*, as well as genes important for neonatal uterine differentiation (*Wnt7a*, *Hoxa10*, and *Msx2*), were severely disrupted on PND5 in GEN-exposed mice.

Discussion: Our findings suggest that neonatal GEN exposure in mice disrupts expression of genes important for uterine development, causing posteriorization and diminished gland function during pregnancy that contribute to implantation failure. These findings could have implications for women who consumed soy-based formulas as infants. https://doi.org/10.1289/EHP6336

Introduction

Developmental exposure to estrogenic chemicals is associated with abnormalities in the female reproductive tract that lead to infertility and cancer in women and in mouse models (Reed and Fenton 2013). Phytoestrogens, or plant-derived estrogenic compounds, are a group of environmentally relevant chemicals that exert estrogenic activity. A major source of phytoestrogens in the diet is the isoflavones found in soy (Kurzer and Xu 1997). Survey studies estimating the amount of soy protein and isoflavones consumed per day by Asian adults suggest an intake of 6–11 g of soy protein of which 25–50 mg is isoflavones (Messina et al. 2006), an approximate isoflavone exposure of <1 mg/kg per day. In a small study ($n = 194$) of adult Asian-American women, the participants were found to have serum circulating levels of isoflavones of <100 nM (Wu et al. 2004). The most prevalent isoflavone in human exposures is genistein (GEN), which makes up approximately 65% of the isoflavone content in soy products (Adlercreutz and Mazur 1997; Kurzer and Xu 1997). In a small study of British women ($n = 100$) split into four groups ranging from no soy intake to high soy intake, the participants were found to have circulating levels of GEN from 14.3 to 378 nM (Verkasalo et al. 2001). A much higher exposure to isoflavones occurs in human infants fed soy-based infant formulas, with estimates of around 10 mg/kg per day in one small study (Setchell et al. 1997). The high intake of soy isoflavones in human infants most likely results in higher exposure rates than in adults. Supporting this statement, a small study of human infants fed exclusively soy-based infant formula had serum circulating levels of GEN (1–10 μM), which is at least 10-fold higher than any natural exposure of adults (Cao et al. 2009; Setchell et al. 1997).

A mouse model of developmental phytoestrogen exposure was described previously where neonatal CD-1 female pups were exposed to GEN at 50 mg/kg per day by subcutaneous injection (Doerge et al. 2002). This dosing strategy produced serum circulating levels that closely approximated the levels measured in a study with human infants consuming soy-based infant formula (Cao et al. 2009). In this model system, female mice exposed neonatally to GEN were infertile (Jefferson et al. 2005), and 35% of the mice developed uterine cancer later in life (Newbold et al. 2001). A hallmark of this cancer is abnormal cellular differentiation characterized by distinct basal cell populations that express proteins normally restricted to the cervix and upper vagina (Suen et al. 2016, 2018). This phenotype is consistent with our findings of posteriorization in the oviduct of GEN-exposed mice (Jefferson et al. 2011). Reproductive tract posteriorization has been described in mouse models with deletions of important uterine patterning genes, most notably the *Hoxa* and *Wnt* gene families (Du and Taylor 2015; Franco et al. 2011; Hayashi et al. 2011). These data suggest that neonatal exposure to GEN alters female reproductive tract differentiation and leads to a molecular signature resembling patterning gene deletions.

GEN-exposed mice exhibit complete infertility for multiple reasons, including abnormal function of the hypothalamic–pituitary–gonadal axis, leading to ovulation failure and abnormal estrous

Address correspondence to Wendy N. Jefferson, NIEHS/NIH/DHHS, P.O. Box 12233, MD E4-05, Research Triangle Park, NC 27709 USA. Email: jeffers1@niehs.nih.gov

Supplemental Material is available online (https://doi.org/10.1289/EHP6336).
The authors declare they have no actual or potential competing financial interests.
Received 3 October 2019; Revised 5 February 2020; Accepted 8 February 2020; Published 18 March 2020.

cycling, deficits in oviductal support of preimplantation embryo development, and failure of embryo development following implantation (Jefferson et al. 2005, 2009). Implantation is a complex process orchestrated by a carefully timed series of estrogen and progesterone signals (Lee et al. 2007; Spencer 2014). These hormonal signals drive endometrial proliferation, which is followed by endometrial differentiation events that create a short window of implantation during which the endometrium can support invasion by the embryo. Glands within the endometrial stroma produce factors required for implantation such as enzymes, transporters, and secreted proteins. One of the most important factors is leukemia inhibitory factor (LIF), without which implantation does not occur (Salleh and Giribabu 2014; Stewart et al. 1992). Upon embryo implantation, the uterine stroma undergoes decidualization, during which the stromal cells expand and differentiate to support the fetal–maternal interface required for proper embryo development.

Complex hormonal signaling and precise timing of endometrial proliferation and differentiation events are crucial for successful embryo implantation and growth, but how neonatal GEN exposure disrupts this process is unknown. Here we comprehensively examined the mechanisms underlying neonatal GEN-exposure–induced deficits in uterine support for implantation.

Material and Methods

Animals

Timed-pregnant CD-1 mice were obtained from the in-house National Institutes of Health/National Institute of Environmental Sciences (NIH/NIEHS, Research Triangle Park, NC) breeding colony. Mice were handled under approved animal care and use protocols according to NIH/NIEHS guidelines. Mice were fed NIH-31 diet and housed in a temperature-controlled environment (21–22°C) with a 12-h light:12-h dark cycle. At birth, postnatal day 1 (PND1), pups were randomly standardized to 10 female pups per dam. Female pups were treated by subcutaneous injection of 0.02 mL of corn oil [control (CON); Spectrum; Catalog No. CO136] or GEN (Sigma; Catalog No. G6649) dissolved in corn oil at 50 mg/kg per day on PND1 through PND5, as described previously (Jefferson et al. 2005). The corn oil used in this study was confirmed to have no detectable estrogenic activity in a uterotrophic bioassay, as previously described (Jefferson et al. 2002). Uterine tissues were collected on PND5, 4 h after the last injection or the mice were weaned at PND21 and housed five per cage. Uteri were collected at various time points detailed in subsequent "Methods" sections. At 6–8 weeks of age, females were either ovariectomized for hormone response assays, superovulated and bred, or naturally bred for prepregnancy and early pregnancy end points. Of note, all females used for natural breeding time points in this study were 6 weeks of age. GEN-exposed mice do not become anovulatory until later in life (at $\sim$4 months of age) (Jefferson et al. 2005). Superovulation was accomplished by subcutaneous injection of 5 IU equine chorionic gonadotropin (eCG; Sigma; Catalog No. E4877) in 0.1 mL saline followed 48 h later with 5 IU human chorionic gonadotropin (hCG; EMD Millipore; Catalog No. 230734) in 0.1 mL saline. A small group of superovulated mice was used for serum collection 24 h post hCG treatment without breeding. For early pregnancy end points, superovulated females or naturally bred females were placed with proven fertile males and the presence of a vaginal plug was used as a determination of pregnancy and considered gestational day (GD) 0.5. For intact mice at 2 months of age, uteri were collected and the estrous cycle stage determined by vaginal cytology. The number of mice used for each experiment is detailed in each "Methods" section below.

Mice with conditional deletion of *Foxa2* in the uterus were generated by crossing *Foxa2*-floxed mice (Stock No. 022620; Jackson Laboratory) with *Pgr*-cre mice (from F. DeMayo, NIEHS, Research Triangle Park, NC) (Soyal et al. 2005). Mice that were flox/flox, cre$^-$ served as wild-type controls (*Foxa2* WT), whereas littermates that were flox/flox, cre$^+$ were lacking *Foxa2* in the uterus (*Foxa2* cKO). Housing and weaning were as described above. At 2 months of age, *Foxa2* WT and *Foxa2* cKO female mice were bred to *Foxa2* WT males until the detection of a vaginal plug. Only vaginal plug–positive mice were used in the experiments described below.

Whole-Mount Immunofluorescence

Uteri were collected from female mice (CON and GEN; $n = 10$ per group) at 26 d of age (prior to establishment of estrous cyclicity) and immediately fixed in dimethyl sulfoxide:methanol (1:4 ratio) and stored at −20°C until processing. Immunofluorescence was carried out, as previously described (Arora et al. 2016). In brief, tissues were blocked using 2% powdered milk and 1% Triton™ X-100 in phosphate buffered saline (PBS) for 2 h at room temperature (RT). Primary antibodies for mouse CDH1 (Clontech; Catalog No. M108) and FOXA2 (Abcam; Catalog No. ab108422) were diluted (1:200) in block, and uteri were incubated for 5 d at 4°C. Uteri were washed (PBS + 1% Triton) six times for 30 min each and incubated with secondary antibodies, fluorescently conjugated Alexa Fluor IgGs (1:500), donkey anti-rabbit (Invitrogen; Catalog No. A31572), and goat anti-rat (Invitrogen; Catalog No. A21247) for 2 d at 4°C. Uteri were washed (1% Triton™ X-100 in PBS) six times for 30 min each, dehydrated in methanol, and incubated overnight in 3% hydrogen peroxide diluted in methanol. Uteri were washed in 100% methanol twice for 15 min each and cleared overnight using benzyl alcohol:benzyl benzoate, 1:2 ratio. Uteri were imaged using a Leica SP8 TCS confocal microscope with white-light laser, using a 10× air objective with *z*-stacks 7 µm apart. Full uterine horns were imaged using tile scans and tiles were merged using the mosaic merge function of the Leica software (version 3.5.5; Leica Microsystems).

Image Analysis

Leica immunofluorescence software files (Leica) were analyzed using Imaris (version 9.2; Bitplane Imaris). Surfaces were created in surpass three-dimensional mode for the CDH1$^+$ lumen signal and the FOXA2$^+$ glandular signal. Gland numbers were determined by number of disconnected components in the FOXA2$^+$ gland surface, as previously described (Arora et al. 2016). Images of the surfaces and the two-dimensional optical slices were captured using the snapshot function.

Hormone Response Assays

The treatment regimen for the hormone response assays is depicted in Figures 1A and 2A. Female mice (CON and GEN) were ovariectomized at 6 weeks of age and allowed to recover for 10–14 d to clear endogenous hormones. The mice were then treated by subcutaneous injection of 0.1 mL of corn oil vehicle (Veh) or one of the following hormone regimens using 17β-estradiol (E2; Sigma; Catalog No. E8875) or progesterone (P4; Sigma; Catalog No. P0130) or a combination of the two as follows: *a*) E2 group; 25 µg/mouse for 2 h or 24 h ($n = 5$ per group); *b*) E2-3X group; E2 25 µg/mouse for three daily injections collected 24 h after the last injection for uterine weight ($n = 5$ per group); *c*) E2 + P4 group; E2 6.7 ng/mouse for 3 d, rest for 2 d, E2 100 ng/mouse + P4 40 mg/mouse for 3 d, collected 24 h after last injection ($n = 5$ per group); *d*) Decidua group; E2 + P4 regimen but 24 h after last dose the uterine horn was infused with corn oil to initiate decidual response, as previously described (Paria et al. 1999). Uteri were collected either 2 h after oil infusion or continued E2 + P4 for 8 consecutive d and then uteri were collected

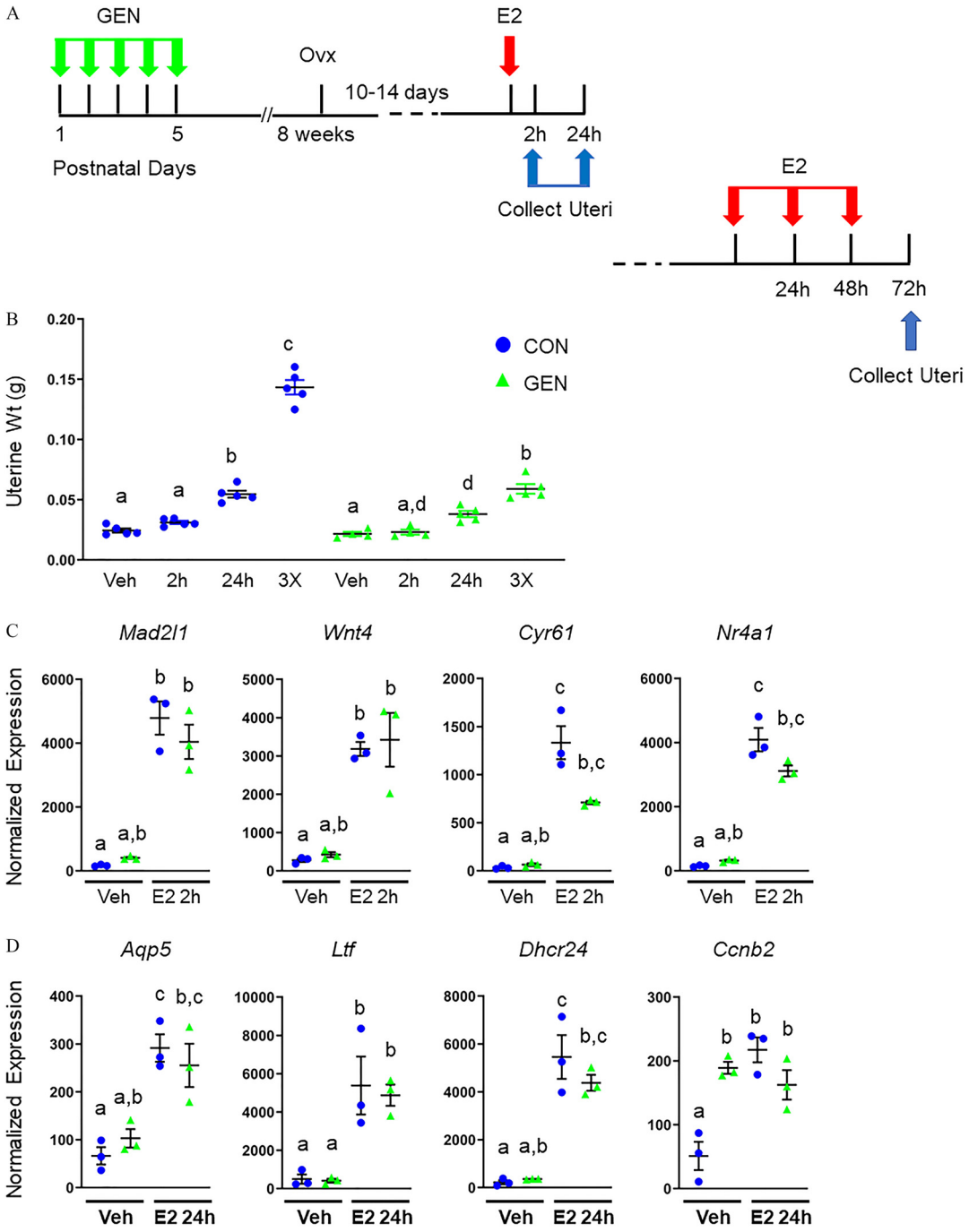

Figure 1. Uterine response to estradiol in genistein (GEN)-exposed mice. (A) Schematic depicting treatment and collection timing for 17β-estradiol (E2) experiments. Each arrow represents a single injection of the chemical indicated above the arrows. (B) Uterine wet weight (in grams) is plotted for each time point [Vehicle (Veh), E2-2h, E2-24h, and E2-3X] for both control (CON) and GEN-exposed mice. (C) Real-time RT-PCR of select E2-regulated genes 2 h post E2 treatment in CON and GEN-exposed mice. (D) Real-time RT-PCR of select E2-regulated genes 24 h post E2 treatment in CON and GEN-exposed mice. Mean ± SEM is plotted along with individual values for all panels. Different letters indicate significance at $p \leq 0.05$ using Kruskal-Wallis test followed by Dunn's test ($n = 3$–5 per group). Note: RT-PCR, reverse transcription polymerase chain reaction; SEM, standard error of the mean.

24 h after the last injection for uterine weight ($n = 20$ per group); and *e*) P4 group; 40 mg/mouse for 6 h or 24 h ($n = 5$ per group). All uteri collected for molecular hormone response assays were frozen at −80°C until further use.

Hormone Assays

Eight-week-old female mice (CON or GEN) were superovulated, as described above in the "Animals" section; half of the mice were bred to proven male breeders and pregnancy confirmed by vaginal plug the next day ($n = 5$–7 mice per group). Blood was collected from the vena cava 48 h after eCG (no hCG; nonpregnant) or 24 h after hCG from vaginal plug–positive mice (pregnant); uteri were also collected and frozen at −80°C at both time points. Blood was allowed to clot for 1 h at RT and then centrifuged at 8,000 × *g* at 4°C for 10 min to isolate serum. E2 and P4 serum levels were measured using respective radioimmunoassay kits (Diagnostic Systems Laboratory: P4, Catalog No. DSL 3400; E2, Catalog No. DSL 4400) according to the manufacturer's instructions.

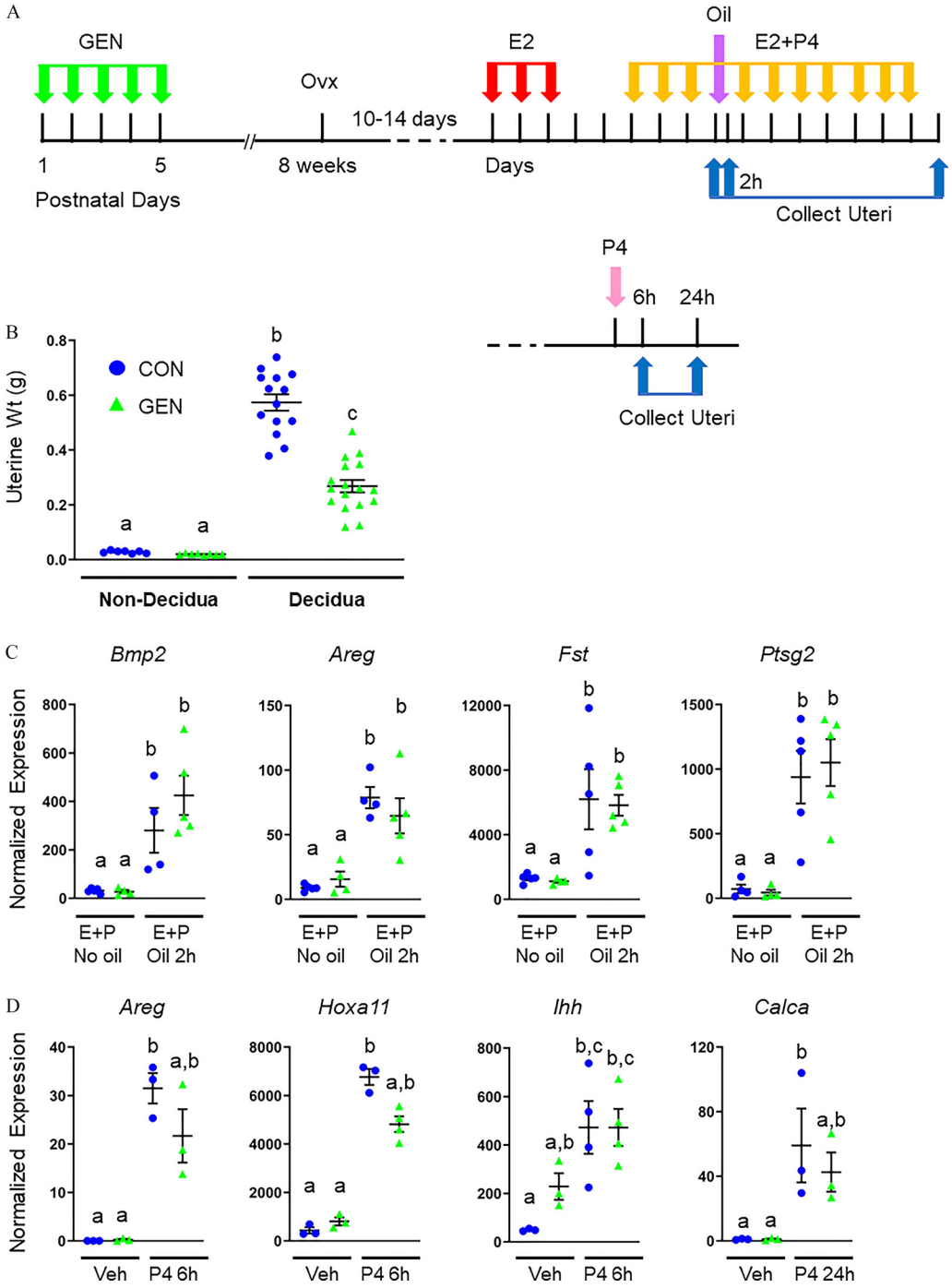

Figure 2. Decidual response in GEN-exposed mice. (A) Schematic depicting treatment and collection timing for decidua experiments (top) and progesterone (P4) experiments (bottom); events prior to the dashed line are the same for each group. Each arrow represents a single injection of the chemical indicated above the arrows. Uterine tissue collection time points are indicated by an arrow. (B) Uterine weight (in grams) in non–oil-infused horn and oil-infused horn with decidual response in CON and GEN-exposed mice. (C) Real-time RT-PCR of select decidual response genes without oil infusion or 2 h following oil infusion. (D) Real-time RT-PCR of select progesterone-regulated genes 6 h and 24 h after P4 treatment. Mean ± SEM is plotted along with individual values for all panels. Different letters indicate significance at $p \leq 0.05$ using Kruskal-Wallis test followed by Dunn's test ($n = 7$–17 per group for A; $n = 3$–5 per group for B and C). Note: CON, control; GEN, genistein; RT-PCR, reverse transcription polymerase chain reaction; SEM, standard error of the mean.

Early Pregnancy and LIF Rescue

Eight-week-old female mice (CON or GEN) were bred to proven male breeders (2:1) until vaginal plug detection (GD0.5). Uteri were collected on GD1.5, GD3.5, GD4.5, or GD5.5 and frozen at −80°C until RNA isolation ($n = 4$ per group). For GD4.5 or GD5.5, vaginal plug–positive mice were given a tail vein injection of Evan's blue dye (1% in 0.1 mL saline) 2–3 min prior to being euthanized to visualize implantation sites; only mice that had confirmed blue implantation sites were used for further analysis. For LIF rescue, vaginal plug–positive CON and GEN females were treated with either saline or LIF (BioLegend; Catalog No. 554008; 10 mg/mouse) in 0.1 mL saline by intraperitoneal injection on GD3.5 ($n = 9$–12 per group). On GD5.5, pregnant mice

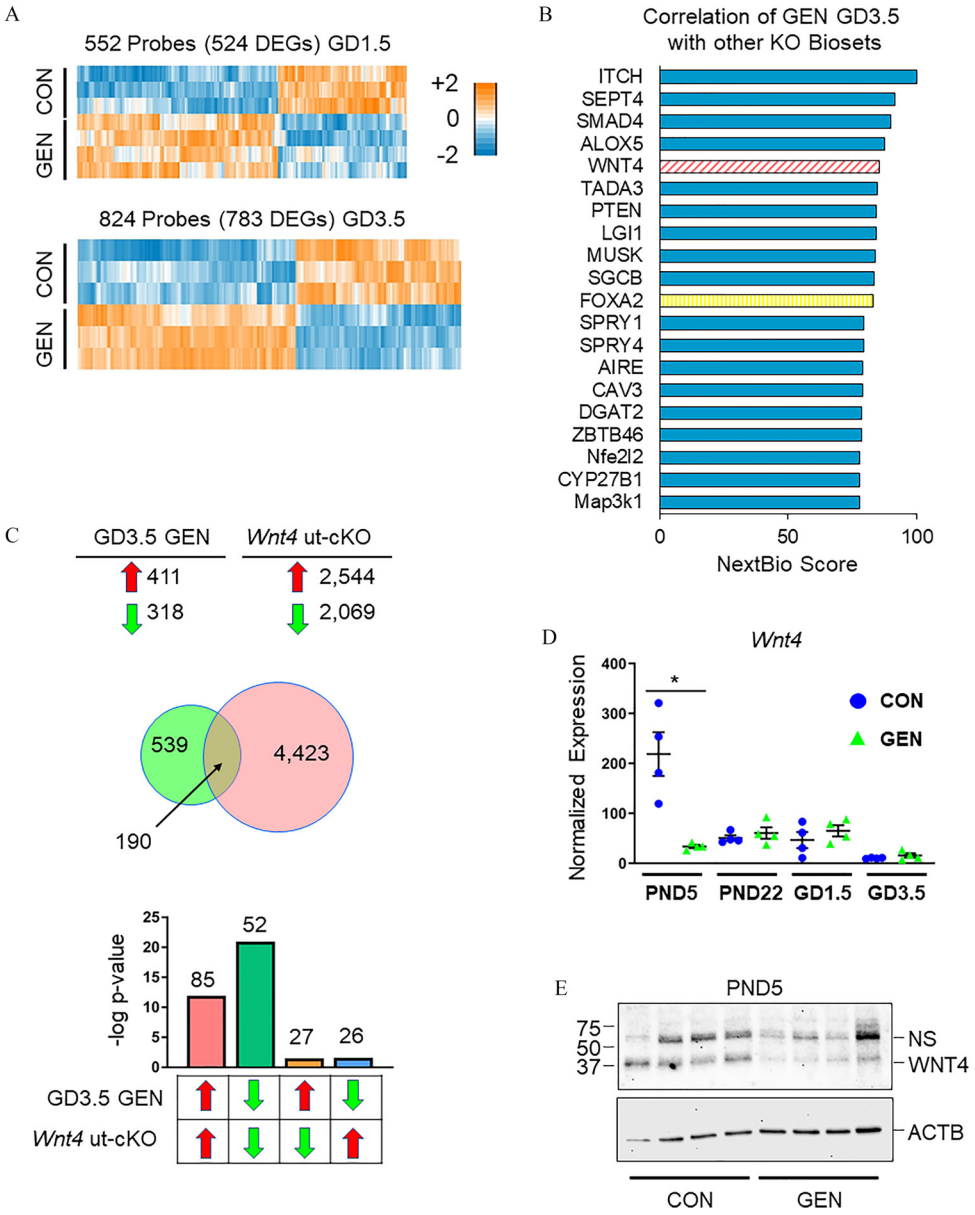

Figure 3. Uterine gene expression in GEN-exposed mice during early pregnancy compared with conditional uterine deletion of *Wnt4*. (A) Microarray analysis of GEN-exposed vs. CON on gestation day (GD) 1.5 (top) and GD3.5 (bottom). Number of differential probes and differentially expressed genes (DEGs) is shown above each clustered heat map. (B) NextBio knockout (KO) atlas overlap of GEN GD3.5 with gene perturbation models plotted in order of NextBio score (select genes of interest in different colors and patterns). (C) NextBio KO atlas comparison of GD3.5 GEN vs. CON uterine data set with *Wnt4* uterine conditional KO (*Wnt4* ut-cKO) uteri vs. wild type on decidualization Day 1 (equivalent to GD3.5). Numbers are the number of genes increased (red arrows pointed up) or decreased (green arrows pointed down) for each group (top). Venn diagram shows the number of overlapping genes between the two data sets (middle). The direction of gene expression overlap is shown in the graph (bottom) with gene expression direction shown under each category for each data set. Number of genes in each category is labeled above each bar. Numbers plotted are the negative-log *p*-value. (D) Real-time RT-PCR of *Wnt4* over time; postnatal day (PND) 5, PND22, GD1.5, and GD3.5. Mean ± SEM is plotted along with individual values. $^{*}p < 0.05$ CON vs. GEN for each time point using Kruskal-Wallis test followed by Dunn's test ($n \geq 3$ per group). (E) Immunoblot of WNT4 in CON and GEN uteri on PND5 ($n = 4$ per group). Molecular weight markers are indicated on the left and the specific band for WNT4 is indicated on the right [nonspecific (NS) band indicated on the right]. ACTB immunoblot is shown below as a loading control. Note: ACTB, β-actin; CON, control; GEN, genistein; RT-PCR, reverse transcription polymerase chain reaction; SEM, standard error of the mean.

were given a tail vein injection of Evan's blue dye and the number of implantation sites were counted; GD9.5 implantation sites were counted without blue dye injection ($n = 6$–7 per group). Implantation sites were counted and imaged. As a positive control for the LIF rescue, 8-week-old female *Foxa2* WT or *Foxa2* ut-cKO mice ($n = 5$–7 mice per group) were bred to *Foxa2* WT males until vaginal plug detection, as previously described (Jeong et al. 2010); LIF injections on GD3.5 rescued implantation failure in *Foxa2* ut-cKO mice on GD5.5 as visualized by Evan's blue dye.

Histopathology and Immunohistochemistry

Uterine tissues collected from PND5 pups, intact mice at 2 months of age, and pregnant mice on GD5.5 were fixed in 10% neutral buffered formalin [0.29 M monosodium phosphate (NaH_2PO_4-H_2O), 0.24 M disodium phosphate (Na_2HPO_4-$7H_2O$), 10% formaldehyde] overnight at 4°C, which was then changed to ice cold 70% ethanol ($n = 3$–5 per group). The tissues were processed, embedded in paraffin, and sectioned at 6 μm. Tissue sections were stained with either hematoxylin and eosin (H&E) or Masson's trichrome stain using

standard protocols or immunostained using standard protocols (Carson and Hladik 2009; Munro 1971). KRT14 immunostaining was performed using the standard avidin–biotin–peroxidase technique previously reported (Suen et al. 2018). In brief, rabbit polyclonal anti-KRT14 antibody (BioLegend; Catalog No. PRB-155P; concentration 0.8 mg/mL) was used as the primary antibody and biotinylated donkey anti-rabbit IgG (Jackson ImmunoResearch; 1:500 dilution) was used as the secondary, and the complex was visualized using 3-diaminobenzidine (DAB) chromagen (Dako). FOXA2 immunostaining was performed following heat-induced antigen retrieval using a Decloaker (Biocare Medical) with 1× ethylenediaminetetraacetic acid pH 8.5 for 15 min at 110°C. Endogenous peroxide was quenched using 3% hydrogen peroxide for 15 min. Sections were incubated with Rodent Block M (BioCare Medical) for 20 min at RT. Rabbit monoclonal anti-FOXA2 (Cell Signaling; Catalog No. 8186S; concentration 1 mg/mL) was applied for 1 h at RT. Tissues were then incubated with Rabbit on Rodent Horse Radish Peroxidase (HRP) Polymer (BioCare Medical; Catalog No. RMR622) for 30 min at RT. Complexes were visualized using DAB.

Protein Isolation and Immunoblotting

PND5 or GD3.5 frozen uterine tissues ($n = 4$ per group) were pulverized on dry ice, and 20 mg of crushed tissue was homogenized by hand-held homogenizer using 200 µL of tissue protein extraction reagent (T-PER™; Invitrogen). Samples were centrifuged at 10,000 rpm for 5 min and the total protein extract was removed from the pellet. Halt Protease and Phosphatase Inhibitor Cocktail (Thermo Fisher; Catalog No. 1861281) was added at 1:100 to prevent protein degradation. The protein concentration was determined using the Qubit protein assay (Life Technologies; Catalog No. Q33212). Twenty micrograms of total protein was electrophoresed on a 4–20% Tris-glycine sodium dodecyl sulfate gel (Bio-Rad) and transferred to a polyvinylidene fluoride membrane (Bio-Rad) using a Trans-Blot turbo (Bio-Rad) for 7 min. Blots were blocked with 5% milk in Tris buffered saline (TBS; Bio-Rad; Catalog No. 1706435) plus 0.1% Tween-20 (TBS-T; Sigma; Catalog No. P1379) for 1 h at RT and then primary antibodies applied overnight at 4°C. The primary antibodies were diluted in 5% milk in TBS-T at the following concentrations: anti-FOXA2 (0.20 µg/mL); anti-SOX17 (1.0 µg/mL; R&D; Catalog No. AF1924); anti-WNT4 (0.5 µg/mL; R&D; Catalog No. AF475). Blots were washed 3 × 15 min in TBS-T and the appropriate peroxidase-conjugated secondary antibody diluted in 1% milk in TBS-T was applied for 1 h at RT: anti-rabbit (0.032 µg/mL; Jackson Immunoresearch; 711-035-152); anti-goat (0.032 µg/mL; Jackson Immunoresearch; 805-035-180); anti-mouse (1:10,000; GE Healthcare; Catalog No. NA931V). Blots were washed 3 × 15 min with TBS-T. Blots were incubated

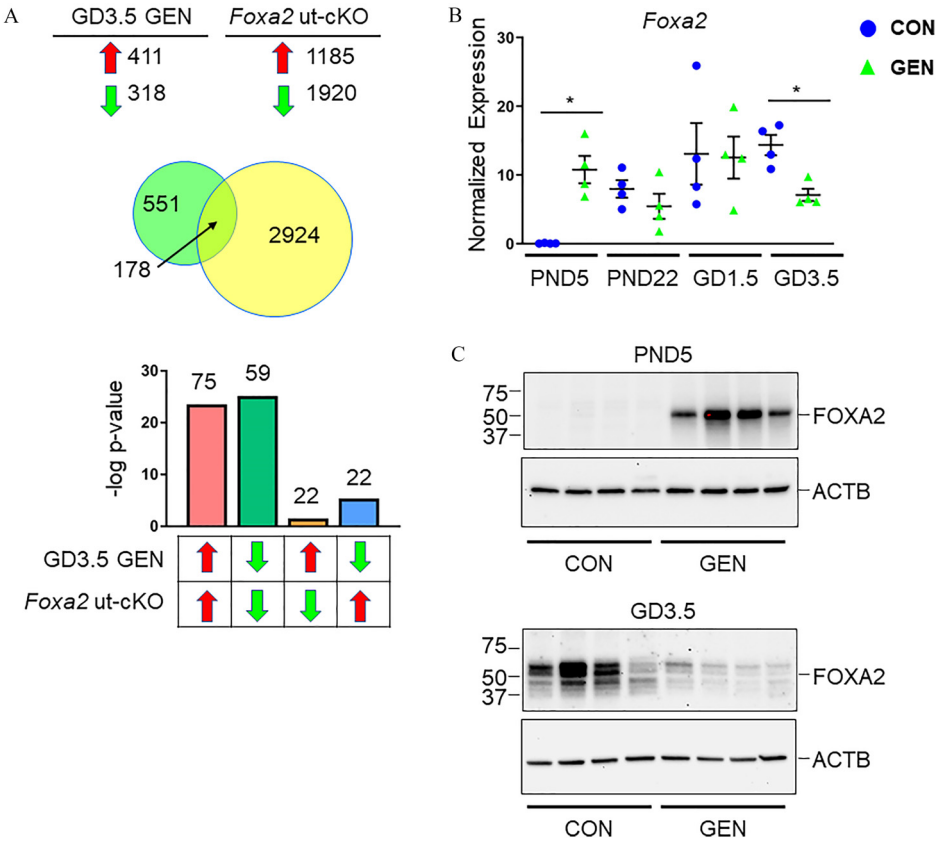

Figure 4. Uterine gene expression in GEN-exposed mice during early pregnancy compared with conditional uterine deletion of *Foxa2*. (A) NextBio knockout (KO) atlas comparison of GD3.5 in GEN-exposed vs. CON uterine data set with *Foxa2* ut-cKO uteri vs. wild type on decidualization Day 1 (equivalent to GD3.5). Numbers are the number of genes increased (red arrows pointed up) or decreased (green arrows pointed down) for each group (top). Venn diagram shows the number of overlapping genes between the two data sets (middle). The direction of gene expression overlap is shown in the graph (bottom) with gene expression direction shown under each category for each data set. Number of genes in each category are labeled above each bar. Numbers plotted are the negative-log *p*-value. (B) Real-time RT-PCR of *Foxa2* over time; PND5, PND22, GD1.5, and GD3.5. Mean ± SEM is plotted along with individual values. $^{*}p \leq 0.05$ using Kruskal-Wallis test followed by Dunn's test ($n \geq 4$ per group). (C) Immunoblot of FOXA2 in CON and GEN uteri on PND5 (top panel) and GD3.5 (bottom panel) ($n = 4$). Molecular weight markers are indicated on the left and the specific band for FOXA2 is indicated on the right. ACTB immunoblot is shown below each blot as a loading control. Note: ACTB, β-actin; CON, control; GD, gestational day; GEN, genistein; PND, postnatal day; RT-PCR, reverse transcription polymerase chain reaction; SEM, standard error of the mean.

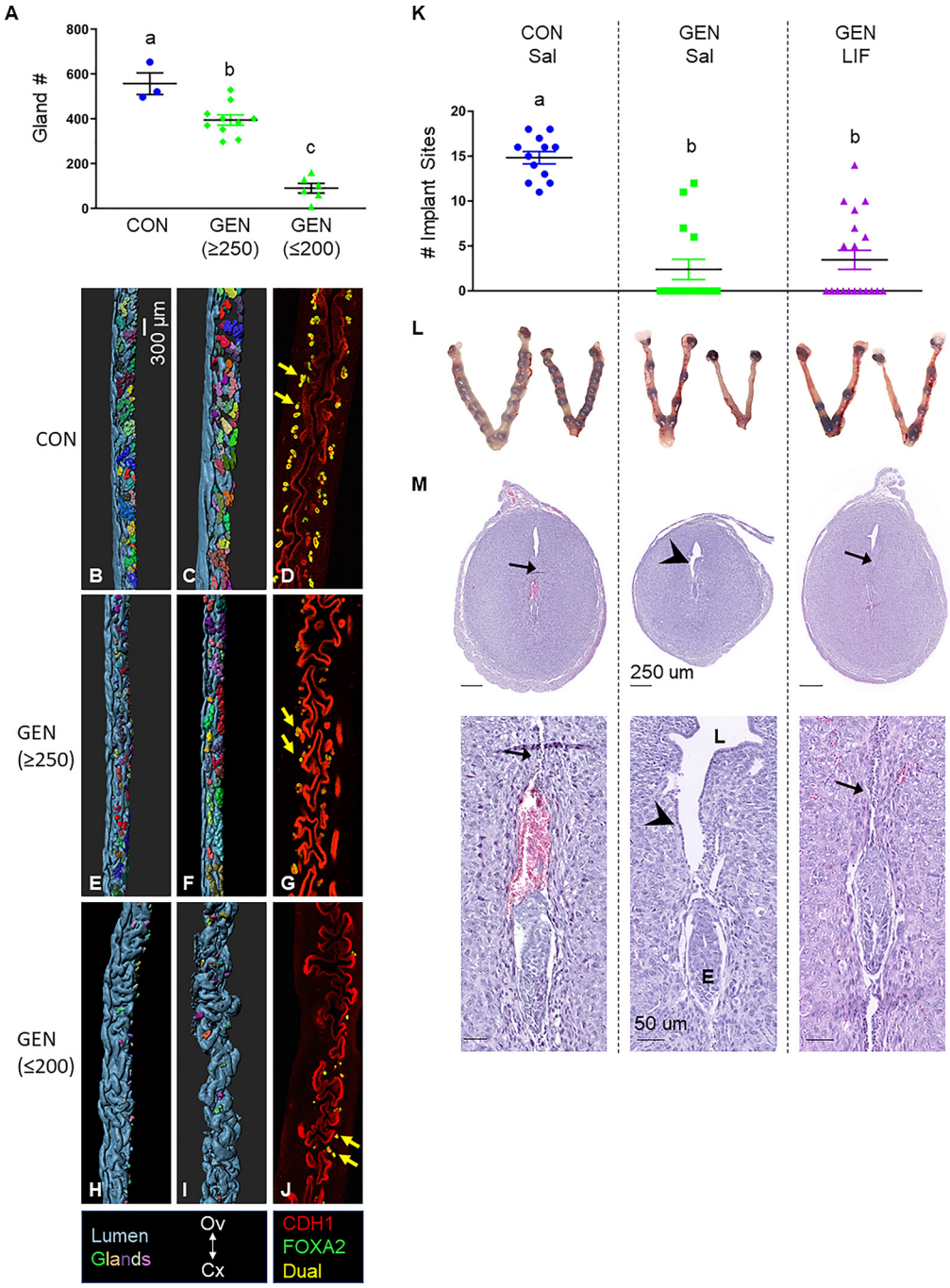

Figure 5. Uterine gland formation and implantation in GEN-exposed mice. (A) Graphical representation of the number of glands in single uterine horns from CON and GEN-exposed mice separated into two groups (GEN ≥250 glands per horn; GEN ≤200 glands per horn). Mean ± SEM is plotted along with individual values. $^{*}p < 0.05$ CON vs. GEN for each time point using Kruskal-Wallis test followed by Dunn's test ($n \geq 3$ per group). (B–J) Representative three-dimensional reconstruction of single uterine horns from CON and GEN-exposed mice on PND26 using Imaris (version 9.2; Bitplane Imaris). Treatment group is indicated on the left. For the left two panels of each group, the lumen is depicted as blue and each individual gland is labeled with a different color. For the right panel of each group, CDH1 immunofluorescence is red, FOXA2 immunofluorescence is green, and the merge of both markers is yellow. (B–C) Normal endometrial gland appearance and distribution in one uterine horn from two individual mice. (E–F) Glands from one horn of two individual GEN-exposed mice with ≥250 glands per uterine horn. (H–I) Glands from one horn of two individual GEN-exposed mice with ≤200 glands per uterine horn. (D,G, and J) Two-dimensional optical slices from C,F, and I, respectively, as represented by CDH1 and FOXA2 immunofluorescent staining. Colors of pseudocolor or immunofluorescence are indicated in the legend. Scale bar: 300 μm (shown in B). All panels are oriented as indicated in legend with ovary (Ov) toward the top and cervix (Cx) toward the bottom. For panels B,E, and H, mesometrial (M)–anti-mesometrial (AM) orientation is left to right, and for panels C,D,F,G,I, and J, M-AM orientation is in and out of the plane of the paper. Yellow arrows indicate examples of dual-labeled gland cells. (K) Implantation site number per uterus is plotted with Mean ± SEM for CON + Saline (CON Sal), GEN + Saline (GEN Sal), and GEN + LIF (GEN LIF) groups as indicated. Different letters represent statistical significance at $p < 0.01$ using ANOVA followed by Dunn's test ($n = 12$–19 per group). (L) Representative gross uteri stained with Evan's blue following tail vein injection from CON Sal, GEN Sal, and GEN LIF groups as indicated above in K (two uteri are shown for each group). Each blue spot indicates an implantation site. (M) Representative cross sections of implantation sites are shown below each group of uteri as indicated in K; low power above and high power of same section below. Notice the open epithelium in the GEN Sal group (indicated by arrowhead) and the lack of opening in the CON Sal and GEN LIF groups (indicated by arrows). Scale bar size is indicated for each row. Note: ANOVA, analysis of variance; CON, control; E, embryo; GEN, genistein; L, lumen; PND, postnatal day; SEM, standard error of the mean.

with Super Signal West Femto Chemiluminescent Substrate (Thermo Fisher; Catalog No. 34095) and visualized using the ChemiDoc Touch Imaging System (Bio-Rad). All blots were stripped using Restore Western Blot Stripping Buffer (Thermo Fisher; Catalog No. 21059). Beta-actin immunoblotting was performed as a loading control, as described above, using anti-β-actin (anti-ACTB; 2 μg/mL; Sigma; Catalog No. A1978) and then HRP-conjugated anti-mouse (1:10,000; GE Healthcare; Catalog No. NA931V). ACTB blots were visualized using Super Signal West Pico Chemiluminescent Substrate (Thermo Fisher; Catalog No. 34087) and the ChemiDoc Touch Imaging System (Bio-Rad).

RNA Isolation and Microarray

Frozen uteri from CON- and GEN-exposed mice from PND5, PND22, hormone response assays, and early pregnancy were pulverized on dry ice and total RNA isolated using the Qiagen RNeasy kit and DNaseI cleanup kit on the column (Qiagen; Catalog Nos. 74104 and 79254) ($n = 3$–5 per group). For real-time reverse transcription polymerase chain reaction (real-time RT-PCR), 1 μg RNA was reverse transcribed to make complementary DNA (cDNA) using the First Strand Synthesis kit (Invitrogen; Catalog No. 11904) following the manufacturer's instructions. Real-time RT-PCR was performed using 20 ng cDNA, 2X SYBR green (Thermo Fisher; Catalog No. 4367659), and primers designed using Primer 3 Express (Koressaar and Remm 2007) using an Applied Biosystems Step One Plus real-time PCR machine with standard settings (Thermo Fisher). A list of primers (Sigma) can be found in the Supplemental Material in Excel File 1.

For microarray analysis, total RNA was isolated from uterine tissues ($n = 4$ per group) using the RNeasy Mini Kit and RNase free DNase set (Qiagen; Catalog Nos. 74104 and 1080901). Microarray was performed using Agilent Whole Mouse Genome 4×44 multiplex format oligo arrays (Agilent Technologies), as previously described (Jefferson et al. 2011). Differentially expressed genes were determined by the Genomics Suite Gene Expression workflow of Partek software package (version 6.6; Partek). To identify differentially expressed probes, a raw data cutoff of <10 and $\log_2$-transformed analysis of variance (ANOVA) with unadjusted $p < 0.05$ was applied to determine if there was a statistical difference between the means of the groups. The resulting significantly altered genes were subjected to a ± 1.5-fold change cutoff and used to generate heat maps in Partek and were uploaded into the NextBio Correlation Engine (http://www.nextbio.com/b/nextbio.nb; Illumina) for pathway enrichment and correlation to published studies. Published studies that exhibited high overlap with our data sets in NextBio and used to generate data are referenced in the relevant "Results" sections. All experiments were performed with at least three independent uterine samples from individual mice. Array data have been deposited in the Gene Expression Omnibus (GEO accession no. GSE138500).

Statistics

All statistical analyses were performed using GraphPad Prism (version 8.2.1; GraphPad Software). For uterine weight and serum hormone levels, a one-way ANOVA was performed, followed by Tukey's multiple comparison test. For real-time RT-PCR data with multiple comparisons, a Kruskal-Wallis test was performed, followed by uncorrected Dunn's test; each time point was independently collected. For real-time RT-PCR on uterine gland gene expression, a Mann-Whitney one-tailed test was performed (only testing for anticipated decrease). For the number of implantation sites per mouse in the LIF rescue experiment, a Kruskal-Wallis test was performed, followed by Dunn's test, and for the number of mice exhibiting pregnancy, a chi-square analysis was performed. For all tests, $p \leq 0.05$ was considered significant. All raw data for this manuscript can be found in the Supplemental Material in Excel File 2, with each tab containing the raw data used to generate a specific figure.

Results

Estrogen Response in GEN-Exposed Mice

We hypothesized that neonatal GEN exposure impaired implantation by disrupting estrogen signaling responses in the adult uterus. To test this idea, we performed a standard uterine wet weight assay on ovariectomized CON and GEN-exposed mice; the experimental design is depicted in Figure 1A. CON mice treated with E2 for 24 h (CON E2-24h) or E2 daily for 3 d (CON E2-3X) showed the expected significant increase in uterine wet weight compared with CON treated with corn oil vehicle (CON Veh) (Figure 1B). GEN-exposed mice also had a significant increase in uterine weight at these time points (GEN E2-24h and GEN E2-3X) compared with GEN Veh, but that response was dampened compared with CON mice (Figure 1B). Despite this dampened response, select estrogen-regulated genes (Hewitt et al. 2015) were not different between CON and GEN-exposed mice at 2 h or 24 h post E2 treatment (Figure 1C,D; see also Figure S1A,B). For example, *Ltf* exhibited the normal pattern of enhanced induction of expression following E2 treatment, with approximately 10-fold increases in both CON and GEN at 24 h and approximately 5,000-fold increases in both CON and GEN after 3 d of treatment (see Figure S1C). One exception was the overexpression of *Ccnb2* in the GEN Veh group compared with CON Veh; however, there was no difference observed between the E2-treated CON and GEN groups.

Decidualization and Progesterone Responses in GEN-Exposed Mice

Given that proper endometrial decidualization is required for successful implantation, we next tested whether neonatal GEN exposure impacted this response. Female CON and GEN-exposed mice were ovariectomized and then treated with a standard regimen of hormones and intrauterine oil infusion to elicit artificial decidualization; the experimental design is shown in Figure 2A (Paria et al. 1999). CON mice had the expected increase in uterine weight in the decidualized horn compared with the non–oil-infused horn (Figure 2B). Although GEN-exposed mice exhibited an increase in weight of the decidualized horn, the increase was significantly dampened compared with CON mice (Figure 2B). However, select characteristic gene expression changes induced by decidualization were not altered in GEN-exposed mice compared with CON mice (Figure 2C). In addition, well-characterized P4-responsive genes showed similar increases in both CON and GEN-exposed mice (Figure 2D).

Serum Circulating Hormone Levels in GEN-Exposed Mice

To determine if implantation failure could result from alterations in circulating hormone levels, we measured serum levels of E2 and P4. Because the GEN-exposed mice were previously shown to have irregular cycles and only 50–60% of mice showed signs of pregnancy following vaginal plug detection (Jefferson et al. 2005), we measured hormone levels in synchronized superovulated mice. As expected, serum E2 was highest 48 h post eCG and lower 24 h post hCG in pregnant mice, but there was no difference between CON and GEN groups (see Figure S2A). Serum P4 showed the

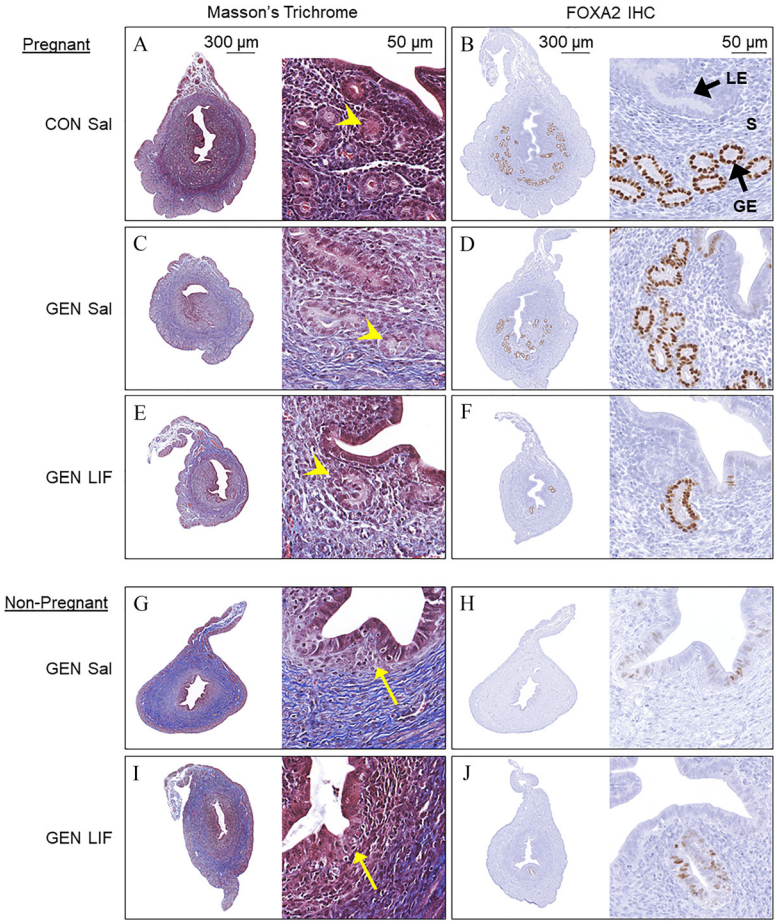

Figure 6. Uterine epithelial and stromal features in GEN-exposed pregnant and nonpregnant mice with or without LIF treatment. Representative histological cross sections from uteri of CON and GEN-exposed mice in between implantation sites for each pregnant group (vaginal plug–positive with visible implantation sites) or in the middle of the horn for the nonpregnant group (vaginal plug–positive but no visible implantation sites); group indicated on the left side of the panels ($n = 4$ mice per group). (A,C,E,G, and I) Sections were stained with Masson's trichrome (left panels). An entire cross section is shown on the left side of the panel (mesometrium is at the top) and higher power magnification of the same sections are shown on the right side of the panel. The presence of glands is indicated by yellow arrowheads in A,C, and E and disorganized luminal epithelium is indicated by yellow arrows in G and I. Note the abnormal endometrium, absence of glands and excess collagen (blue stain) in nonpregnant GEN-exposed mice when compared with pregnant GEN groups with or without LIF treatment. (B,D,F,H, and J) Sections were immunostained for FOXA2. An entire cross section is shown on the left side of the panel (mesometrium is at the top) and higher power magnification of the same sections are shown on the right side of the panel. Note the presence of many $FOXA2^+$ glands in all pregnant mice compared with nonpregnant mice. Scale bar lengths are indicated at the top of each column. Note: CON, control; GE, glandular epithelium; GEN, genistein; LE, luminal epithelium; S, stroma.

expected increase at 24 h post hCG, but again there was no difference between CON and GEN groups (see Figure S2B).

Uterine Gene Expression in GEN-Exposed Pregnant Mice Prior to Implantation

Carefully timed estrogen and progesterone signaling events are primarily responsible for generating a receptive uterine environment. However, these signaling pathways were not considerably altered in GEN-exposed mice. To determine alternative signaling pathways that could explain the implantation failure, microarray analysis was performed on uteri from CON and GEN-exposed mice prior to implantation (GD1.5 and GD3.5). The differentially expressed genes (DEGs) were then compared with curated microarray data sets (Biosets) using Illumina NextBio correlation engine web interface [now known as BaseSpace (Kupershmidt et al. 2010)] to identify potential upstream regulators whose dysfunction could explain the implantation defects. NextBio determines the correlation between the input DEGs and the Biosets by considering both the genes that are differentially expressed and the directions of altered expression.

Microarray analysis of CON and GEN-exposed mice revealed 524 and 783 DEGs on GD1.5 and GD3.5, respectively (Figure 3A). Complete DEG lists are included in the Supplemental Material in Excel File 3: Tables S3A,B. One available comparison in NextBio correlation engine software is the knockout (KO) atlas, in which the Biosets are DEGs from various gene KO models compared with the relevant wild-type controls. Using the NextBio KO atlas, multiple Biosets were highly correlated with the GEN GD1.5 and GD3.5 DEGs [Figure 3B; see also Excel File 3: Tables S3C,D (each tab in Excel File 3 pertains to DEGs and NextBio data generated from GD1.5 and GD3.5 microarray)]. Of the top 20 gene perturbations with high overlap, we selected gene perturbations with known implantation and decidualization deficits for further comparison (Namiki et al. 2018; Rodriguez et al. 2016).

One highly correlated gene perturbation for both GD1.5 and GD3.5 was *Wnt4*. There was a 20% overlap of GEN GD1.5 and 26% overlap of GEN GD3.5 DEGs with DEGs from Day 1 decidualized uteri (similar timing to GD3.5) from mice with a conditional uterine deletion of *Wnt4* (*Wnt4* ut-cKO; Figure 3C; see also Excel File 3: Tables S3E,F) (Large et al. 2014). The *Wnt4* ut-cKO Bioset DEGs were primarily altered in the same direction

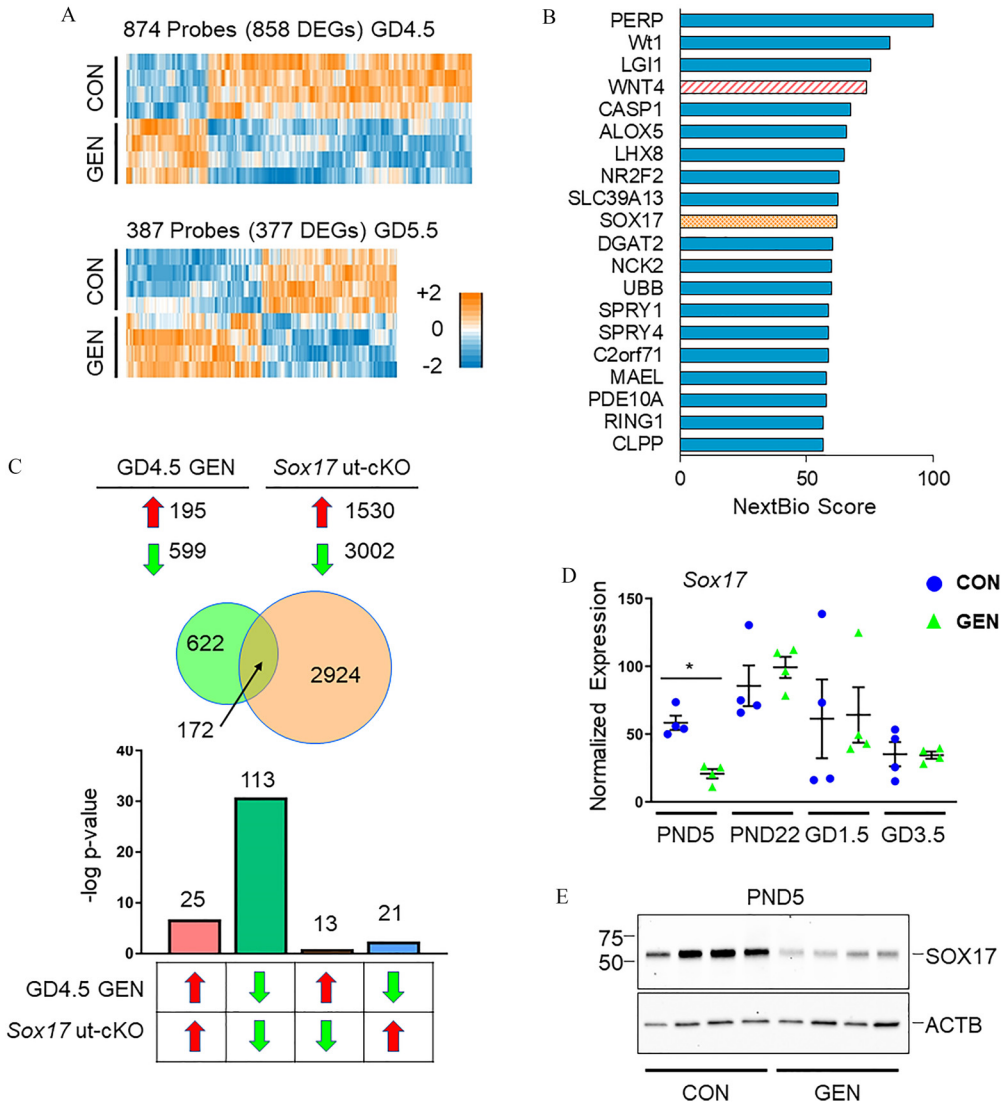

Figure 7. Uterine gene expression in GEN-exposed mice during the window of implantation compared with conditional uterine deletion of *Sox17*. (A) Microarray analysis of GEN vs. CON on GD4.5 (top) and GD5.5 (bottom). Number of differential probes and differentially expressed genes (DEGs) is shown above each clustered heat map using a cutoff of 10 in expression and 1.5-fold change. (B) NextBio knockout (KO) atlas overlap of GEN GD4.5 DEGs with gene perturbation models plotted in order of NextBio score (select genes of interest in different colors and patterns). (C) NextBio KO atlas comparison of GD4.5 GEN vs. CON uterine data set with *Sox17* ut-cKO uteri vs. wild type on GD3.5. Numbers are the number of genes increased (red arrows pointed up) or decreased (green arrows pointed down) for each group (top). Venn diagram shows the number of overlapping genes between the two data sets (middle). The direction of gene expression overlap is shown in the graph (bottom), with gene expression direction shown under each category for each data set. Numbers plotted are the negative-log *p*-value. (D) Real-time RT-PCR of *Sox17* over time; PND5, PND22, GD1.5, and GD3.5. Mean ± SEM is plotted along with individual values. $^{*}p < 0.05$ CON vs. GEN for each time point using Kruskal-Wallis test followed by Dunn's test ($n \geq 4$ per group). (E) Western blot of SOX17 in CON and GEN uteri on PND5 ($n = 4$). Molecular weight markers are indicated on the left and the specific band for SOX17 is indicated on the right. ACTB Western blot is shown below as a loading control. Note: ACTB, β-actin; CON, control; GD, gestational day; GEN, genistein; PND, postnatal day; RT-PCR, reverse transcription polymerase chain reaction; SEM, standard error of the mean.

as seen for GEN GD3.5, suggesting similar altered gene expression patterns in both models. This strong overlap in DEGs would suggest that *Wnt4* may be repressed in the GEN-exposed uterus during early pregnancy; however, *Wnt4* itself was not among the DEGs on GD1.5 or GD3.5 (see Excel File 3: Tables S3A,B). *Wnt4* ut-cKO mice lack *Wnt4* in early pregnancy, but they also lack *Wnt4* during the early neonatal period when *Wnt4* is required for proper uterine patterning (Franco et al. 2011). To investigate whether GEN-exposed mice exhibit reduced *Wnt4* at earlier time points (similar to the *Wnt4* ut-cKO mouse), we performed real-time RT-PCR at several time points. Interestingly, real-time RT-PCR revealed a robust decrease in uterine *Wnt4* expression on PND5 following GEN exposure but not at any other time point examined (Figure 3D). A coordinate decrease in WNT4 protein on PND5 was observed (Figure 3E).

Another gene perturbation from the NextBio KO atlas that highly correlated with the GD3.5 data set was *Foxa2*, which drives endometrial gland development and is critical for implantation (Jeong et al. 2010). There was a 24% overlap of DEGs from the GEN GD3.5 data set with a microarray data set from a mouse model of conditional uterine deletion of *Foxa2* (*Foxa2* ut-cKO) (Figure 4A; see also Excel File 3: Table S3G). Overlapped gene expression was predominantly altered in the same direction as DEGs from *Foxa2* ut-cKO uterine glandular epithelium isolated on pseudopregnant GD3.5 (Filant et al. 2014) (Figure 4A). Two additional data sets of uteri on GD3.5 from *Foxa2* ut-cKO

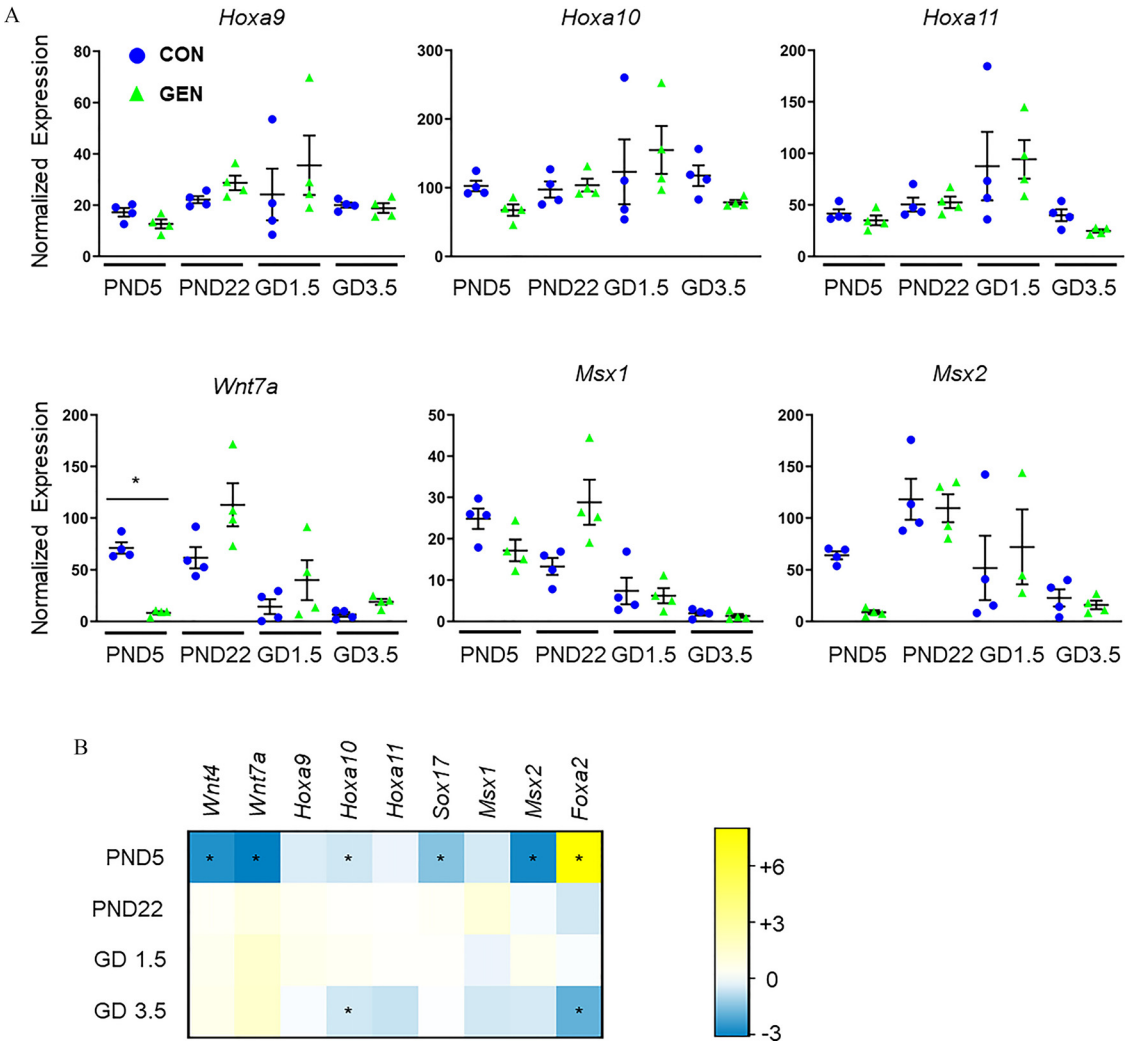

Figure 8. Expression of genes required for female reproductive tract development in CON and GEN-exposed mice. (A) Real-time RT-PCR over time; PND5, PND22, GD1.5, and GD3.5. Gene name indicated above each graph. Mean ± SEM is plotted along with individual values. $^{*}p < 0.05$ CON vs. GEN for each time point using Kruskal-Wallis test followed by Dunn's test ($n \geq 4$ per group). (B) Summary heat map of fold change of each pair of CON and GEN at each time point (listed on the left side) for each gene (listed above the map). Corresponding expression data shown in previous figures: *Wnt4* (Figure 3D), *Foxa2* (Figure 4B), and *Sox17* (Figure 7D). Legend indicating the color representation of the fold change is shown on the right. Asterisk (∗) indicates statistically significant differences in that group described previously. Note: CON, control; GD, gestational day; GEN, genistein; PND, postnatal day; RT-PCR, reverse transcription polymerase chain reaction; SEM, standard error of the mean.

and *Foxa2* conditional deletion only in the uterine epithelium (*Foxa2* epi-cKO) (Kelleher et al. 2018) were compared with the GEN GD3.5 data set and showed similar overlap of GEN-altered genes (see Figure S3A). Real-time RT-PCR assessment of uteri from PND5, PND22, GD1.5, and GD3.5 time points showed increased *Foxa2* gene expression in GEN-exposed mice compared with CON on PND5 during the time of GEN exposure but decreased expression in GEN-exposed mice compared with CON on GD3.5 (Figure 4B). As expected, FOXA2 protein levels were increased in GEN-exposed mice on PND5 but decreased on GD3.5 (Figure 4C). Consistent with this finding, expression of several gland-specific genes on GD3.5 was significantly reduced in GEN compared with CON groups, including *Ttr*, *Prss29*, and *Spink1* (also known as *Spink3*) (see Figure S3B); *Wfdc3* was not significantly different.

Gland Formation in GEN-Exposed Mice

To determine the impact of neonatal GEN exposure on gland formation, we performed whole-mount immunofluorescence and three-dimensional reconstruction of the uterus on PND26, just before the onset of estrous cyclicity (Figure 5A–J). CON mice exhibited normal gland formation with many small glands along the length of the uterine horn. GEN-exposed mice had a significant reduction in gland numbers relative to CON mice (Figure 5A). Of note, the GEN-exposed mice separated into two nonoverlapping groups based on the numbers of glands present. These groups were defined by ≥250 glands per horn or ≤200 glands per horn; both categories were significantly less than in CON mice. The decrease in overall gland number was not a result of gland deficiency in any specific location; the glands that were present appeared to be distributed fairly evenly along the length of the uterine horn (see Figure S4).

Effect of LIF Administration on Implantation Failure Phenotype in GEN-Exposed Mice

To determine if the gland deficits were solely responsible for uterine implantation failure in GEN-exposed mice, we tested whether or not LIF administration could restore implantation, as previously reported for *Foxa2* ut-cKO and *Foxa2* epi-cKO mouse

models (Jeong et al. 2010; Kelleher et al. 2018). We treated vaginal plug–positive CON mice with saline (CON Sal; positive control) and vaginal plug–positive GEN-exposed mice with saline (GEN Sal; negative control) or LIF in saline (GEN LIF) on GD3.5, as previously reported (Jeong et al. 2010). A small group of *Foxa2* ut-cKO mice were treated with LIF on GD3.5 to confirm biological activity and implantation rescue (see Figure S5A). As expected, all CON Sal mice exhibited implantation sites. However, the number of mice in both the GEN Sal and GEN LIF groups that had visible signs of implantation was significantly reduced [CON Sal, 12/12 (100%); GEN Sal, 4/15 (27%); GEN LIF, 8/19 (42%); chi-square analysis, $p < 0.05$]; the two GEN groups were not significantly different from each other. There were also significantly fewer implantation sites in both the GEN Sal and GEN LIF groups compared with the CON Sal group whether the analysis was performed on all mice (Figure 5K) or only mice that had evidence of at least one implantation site (Kruskal-Wallis test followed by Dunn's test, $p < 0.05$). Gross morphology of implantation sites in the uterus was visualized by Evan's blue dye (Figure 5L). Treatment with LIF did not alter the number of implantation sites in the GEN LIF group as compared with the GEN Sal group; however, there appeared to be a significant impact of LIF on the quality of implantation sites (Figure 5M). CON Sal mice had complete uterine epithelial closure around the implanting embryo (6/6 embryos sectioned), demonstrated by direct contact of the epithelium from opposite sides of the lumen on the mesometrial side of the embryo (Figure 5M). However, epithelial closure was not observed in the GEN Sal group (0/6 embryos sectioned) (Figure 5M and Figure S5B). Epithelial closure was partially restored in the GEN LIF group, with 4/6 embryos sectioned exhibiting some epithelial closure. To determine if epithelial closure partially restored by LIF treatment resulted in longer maintenance of pregnancy, a small group of CON Sal, GEN Sal, and GEN LIF mice were collected on GD9.5. LIF did not maintain pregnancy in GEN-exposed mice as evidenced by the number of mice in each group with visible implantation sites [CON Sal, 7/7 (100%); GEN Sal, 2/7 (29%); GEN LIF, 0/6 (0%)], further supporting the idea that implantation failure in GEN-exposed mice is due to multiple mechanisms.

Uterine Histoarchitecture in Pregnant and Nonpregnant GEN-Exposed Mice

Distinct clustering of the GEN mice into two groups with either high or low numbers of glands (GEN $\geq$250 or $\leq$200, as described above) suggests that the variability in successful implantation across the GEN group may be attributed to the number of glands present in individual GEN mice. To determine if this was the case, we compared histological cross sections of uteri from CON and GEN vaginal plug–positive mice with visible implantation sites (pregnant) to GEN vaginal plug–positive mice lacking implantation sites (nonpregnant) on GD5.5. Uterine cross sections from pregnant mice were obtained from interimplantation sites (embryo and decidualized stromal cells were absent from these areas). Sections from nonpregnant mice were collected from the middle of the uterine horn halfway between the cervix and oviduct. CON Sal uteri from pregnant mice exhibited normal endometrial morphology as determined by Masson's trichrome stain (Figure 6A) and H&E (see Figure S6A). All GEN-exposed mice had abnormal endometrial morphology with excessive extracellular matrix (ECM) deposition (Masson's trichrome stain; Figure 6C,E,G,I) and disorganized epithelium (H&E; see Figure S6C,E,G,I). In addition, the glands or gland-like structures observed were abnormal compared with the CON mice in that they were present in low numbers, highly variable in size and shape, and resided close to the primary lumen, suggesting that they were primary luminal folds rather than true functional glands. The stromal compartment was qualitatively reduced in all GEN-exposed mice compared with CON mice and the stromal and muscle compartments appeared to have more ECM accumulation. Regardless of LIF treatment, all GEN-exposed mice exhibited increased collagen deposition (stained blue using Masson's trichrome) when compared with CON Sal mice (Figure 6C,E,G,I). Qualitative assessment of GEN Sal and GEN LIF mice lacking implantation sites indicated a more prominent increase in stromal collagen compared with GEN Sal and GEN LIF mice with implantation sites. Interestingly, abnormal epithelial morphology and stromal composition were prominent features in mice lacking implantation sites as compared with those with implantation sites in both the GEN Sal and GEN LIF groups.

Uterine FOXA2 and KRT14 Expression in Pregnant and Nonpregnant GEN-Exposed Mice

To determine if there was a qualitative difference in glands between the pregnant and nonpregnant groups, FOXA2 immunostaining was performed in tissue sections adjacent to sections stained with Masson's trichrome and H&E. There were numerous small $FOXA2^+$ glands concentrated within the anti-mesometrial side and extending through the depth of the endometrium in CON Sal pregnant uteri (4/4; Figure 6B). All pregnant GEN Sal and GEN LIF uteri had $FOXA2^+$ glands (4/4 for each group; Figure 6D,F), whereas the nonpregnant GEN Sal and GEN LIF uteri lacked $FOXA2^+$ glands or only showed very weak immunostaining (4/4 for each group; Figure 6H,J), suggesting the severity of the gland phenotype plays a role in the implantation failure. Immunostaining of adjacent uterine cross sections with KRT14, a well-characterized basal cell marker, did not reveal the presence of basal cells at this time point (see Figure S6B,D,F,H,J).

Histoarchitecture of GEN-Exposed Mice during the Time of Treatment and in Young Adults

To further characterize the histoarchitecture of GEN-exposed mice, tissue sections from the upper uterus (near oviduct), midbody, and lower uterus (near cervix) on PND5 and in nonpregnant 2-month-old adults were assessed. PND5 CON mice exhibited tubular structure with a simple columnar to cuboidal epithelium and no gland formation throughout the entire length of the uterus (see Figure S7A–C). PND5 GEN-exposed mice exhibited classic features of estrogen exposure, including stromal edema and increased columnar epithelial cell height at all locations examined (Yoshida et al. 1999) (see Figure S7D-F). At 2 months of age, CON mice during the estrus phase of the cycle showed primary luminal folds and small glands at all locations examined (see Figure S7G–I). GEN-exposed mice had shallower primary luminal epithelial folds and variable sized glands with abnormal lumens (often with cribriform features) (see Figure S7J–L). There were no distinguishable differences based on the region of the uterus (near the oviduct vs. near the cervix). In agreement with the lack of KRT14 immunostaining in 6-week-old GEN-exposed pregnant mice, nonpregnant 2-month-old mice in this study did not exhibit characteristic basal or squamous metaplasia in any region of the uterus (0/3 GEN-exposed mice had basal cells).

Uterine Gene Expression in GEN-Exposed Pregnant Mice during the Window of Implantation

Lack of gland formation and function most likely contributes to the implantation failure observed in the majority of GEN-exposed mice. However, these data do not explain why, when implantation does occur in GEN-exposed mice, these embryos still

failed to grow and develop normally. To explore the signaling pathways involved in postimplantation failure, we performed microarray analysis on implantation sites from CON and GEN-exposed mice on GD4.5 and GD5.5. There were 858 DEGs on GD4.5 and 377 DEGs on GD5.5 (Figure 7A; see also Excel File: Tables S4A,B). NextBio comparisons of the GD4.5 and GD5.5 data sets with the KO atlas Biosets revealed several highly correlated gene expression profiles [see Excel File 4: Tables S4C,D (each tab in Excel File 4 pertains to DEGs and NextBio data generated from GD4.5 and GD5.5 microarray)]. Of the top 20 gene perturbations with high overlap, we again selected gene perturbations with known implantation and decidualization deficits for further comparison (Laguë et al. 2010; Namiki et al. 2018; Rodriguez et al. 2016).

Both the GEN GD4.5 and GD5.5 data sets overlapped with the same *Wnt4* ut-cKO Bioset that overlapped with GEN GD1.5 and GD3.5 (see Excel File 4: Tables S4E,F), indicating that the gene expression changes in GEN-exposed mice resembled the *Wnt4* ut-cKO mouse model, independent of stage of pregnancy. We showed above that *Wnt4* expression was significantly decreased in GEN-exposed mice during development but expression did not differ between GEN and CON mice at later time points examined, including early pregnancy (Figure 4D,E). However, multiple genes downstream of *Wnt4* signaling during decidualization, including *Bmp2*, *Fst*, *Ptgs2*, *Wnt6*, *Fkbp4*, and *Fkbp5* (Franco et al. 2011) were not altered in GEN-exposed mice at any pregnancy time point examined (see Excel File 4: Tables S3A,B and S4A,B).

Another highly correlated Bioset in the NextBio KO atlas comparison was *Sox17*, which plays an important role in implantation and decidualization that cannot be rescued by LIF administration (X Wang et al. 2018). There was a 22% overlap of GEN-exposed GD4.5 DEGs and a Bioset from a conditional uterine deletion of *Sox17* on GD3.5 (*Sox17* ut-cKO); the overlapped DEGs were predominantly altered in the same direction (Figure 7C). However, *Sox17* itself was not differentially expressed during pregnancy, nor was *Ihh*, a key downstream signaling molecule of SOX17 (X Wang et al. 2018) (see Excel File 4: Tables S3A,B and S4A,B). These findings highlight the possibility that *Sox17* signaling during early pregnancy is intact in GEN-exposed mice. Interestingly, just as for *Wnt4*, GEN exposure caused a striking reduction in *Sox17* mRNA and protein on PND5 (Figure 7E).

Neonatal Expression of Genes Required for Uterine Development

Based on our findings that three genes (*Foxa2*, *Wnt4*, and *Sox17*) critical for both female reproductive tract development and implantation were disrupted in GEN-exposed mice, we tested whether additional genes with similar KO phenotypes were also disrupted across development and early gestation. The genes examined included *Wnt7a*, *Hoxa9*, *Hoxa10*, *Hoxa11*, *Msx1*, and *Msx2* (Du and Taylor 2015; Hayashi et al. 2009; Nallasamy et al. 2012). Expression of three of these genes (*Hoxa10*, *Wnt7a*, and *Msx2*) was significantly decreased in GEN-exposed mice on PND5 (Figure 8A). A small but significant decrease in gene expression was also observed for *Hoxa10* at GD3.5 (Figure 8A). A summary heat map of the fold changes ($\log_2$ GEN/CON) for these genes along with *Foxa2*, *Wnt4*, and *Sox17* over time clearly demonstrated that the major disruption in gene expression was on PND5, at the end of GEN treatment, but that by PND22, gene expression had largely normalized (Figure 8B). At later time points, only *Foxa2* and *Hoxa10* exhibited a significant decrease in expression in GEN-exposed mice compared with CON mice on GD3.5.

Discussion

Mice exposed neonatally to GEN exhibit defects in embryo implantation in the uterus during early pregnancy. We show herein, that abnormally high expression of *Foxa2* during neonatal uterine differentiation most likely contributes to this phenotype because GEN-exposed mice have disrupted endometrial gland formation and subsequent implantation failure similar to that observed in the *Foxa2* uterine overexpression mouse model (*Foxa2* ut-cOE) (P Wang et al. 2018). *Foxa2* ut-cOE mice also develop the appearance of stratified epithelium by 4 weeks of age (P Wang et al. 2018), but we did not observe a comparable metaplastic change in young adult GEN-exposed mice (6–8 weeks of age) that could account for implantation failure. However, stratified epithelium and basal cell metaplasia are prominent features of GEN-exposed mice later in life, by 6 months of age, suggesting an underlying commonality between these two model systems (Suen et al. 2018). A second contributor to this phenotype was the repression of multiple genes critical for appropriate uterine patterning and differentiation specifically during neonatal development. Mis-regulation of these genes leads to uterine posteriorization, which is characterized by high levels of collagen deposition, indicating abnormal uterine ECM composition and architecture more similar to that normally observed in the uterine cervix and gene expression patterns typical of the cervix and vagina (Kurita et al. 2001). It is not known whether *Foxa2* acts upstream of these developmental patterning genes, particularly during neonatal differentiation of the uterus, or if GEN exposure independently alters them to converge on similar uterine phenotypes. Together with our previous observations of neonatal GEN-induced posteriorization of the oviduct and consequent failure to support preimplantation embryo development in mice (Jefferson et al. 2009, 2011), these mechanisms can explain why the GEN-exposed female reproductive tract is unable to support pregnancy.

It is well established that endometrial gland function is essential for implantation. In the mouse, uterine gland formation begins on PND5 and is complete by PND15 (Cooke et al. 2013). Gland formation can be completely disrupted by exposure to the potent synthetic estrogen, diethylstilbestrol (DES), or by exposure to progesterone during this time period (Cooke et al. 2012; Filant et al. 2012; Yoshida et al. 1999). Similarly, neonatal progesterone exposure results in failure of gland formation in sheep (Gray et al. 2000). In all of these models, the absence of normal glands results in implantation failure, demonstrating the importance of functional glands in establishing pregnancy. FOXA2 is a key mediator of gland formation, with restricted temporal expression resulting in normal gland development and function. In the absence of *Foxa2* in cKO mouse models, glands do not form and mice are infertile due to a lack of LIF secretion (Kelleher et al. 2017). Several genetic mouse models that report a lack of uterine gland formation, including conditional uterine deletions of *Wnt7a*, *Sox17*, and *Wnt4*, also exhibit decreased *Foxa2* expression, suggesting there is a complex signaling network that governs gland formation (Cooke et al. 2013; Guimarães-Young et al. 2016). The converse is also problematic. When *Foxa2* is overexpressed in mice in all uterine cell types beginning in the neonatal period, there are also very few endometrial glands as well as complete infertility, but with the additional appearance of squamous metaplasia, as described above (P Wang et al. 2018). Similarly, the robust increase in FOXA2 in GEN-exposed mice on PND5 likely explains the diminished gland numbers that contribute to implantation failure. If lack of gland function were completely responsible for the implantation deficits, then LIF replacement should have restored implantation in GEN-exposed mice as has been observed in *Foxa2* ut-cKO mice (Kelleher et al. 2018). However, although LIF improved the apparent quality of the implantation sites, there was no rescue of

embryo development, prompting us to investigate additional mechanisms.

Female reproductive tract differentiation occurs in the anterior-to-posterior (AP) direction under the influence of the *Hox* genes (Du and Taylor 2015). The patterning of *Hox* gene expression initiates epithelial and mesenchymal developmental cues that correspond with the appropriate location in the tissue to produce a fully developed and functional organ. For example, development of simple single-layered glandular epithelium is initiated in the uterus but not in the vagina, where stratified epithelium normally develops (Kurita et al. 2001). AP differentiation is driven by *Hoxa9* in the oviduct, *Hoxa10* in the uterus, *Hoxa11* in the lower uterus and cervix, and *Hoxa13* in the cervix and upper vagina (Du and Taylor 2015; Taylor et al. 1997). *Hoxc9-11* and *Hoxd9-11* have some functional redundancy with *Hoxa9-11* (Du and Taylor 2015; Mucenski et al. 2019; Raines et al. 2013). Disruption of *Hoxa10* or combined disruption of *Hoxa9-11* causes posteriorization of the reproductive tract with the anterior movement of stratified epithelium, including basal cells and extracellular matrix, from the cervix and upper vagina up into the uterus (Benson et al. 1996; Mucenski et al. 2019; Raines et al. 2013). Neonatal GEN-exposed mice exhibited all of these characteristics and, in the uterus, expressed genes normally restricted to the cervix and upper vagina, including *Trp63*, *Krt14*, and *Six1* (Suen et al. 2016, 2018). In the present study, GEN-exposed mice had significantly reduced levels of *Hoxa10* and *Hoxa11* in the uterus during neonatal development, which explains, at least in part, the altered AP patterning-associated reproductive tract phenotype observed in this model.

Wnt genes play a role in both AP and radial patterning of the female reproductive tract in part through reciprocal positive feedback interactions with *Hox* genes (Mucenski et al. 2019). Mice lacking *Wnt7a* in the uterus have disorganized muscle layers, do not form glands, exhibit postnatal down-regulation of *Hoxa10*, *Hoxa11, Msx1*, and *Msx2* and are posteriorized with the appearance of stratified epithelium (Dunlap et al. 2011). *Wnt7a* is also required to restrict another patterning gene, *Wnt4*, to the neonatal stromal and myometrial layers given that mice lacking *Wnt7a* exhibit aberrant uterine epithelial expression of *Wnt4*. Although total uterine *Wnt4* expression was not changed in *Wnt7a* ut-cKO mice, we observed down-regulation of both *Wnt7a* and *Wnt4* in GEN-exposed mice on PND5. These findings are in agreement with previous studies of postnatal DES exposure in which *Wnt7a* is reduced and *Wnt4* is reduced and redistributed to the epithelium on PND5 (Carta and Sassoon 2004; Hayashi et al. 2011; Miller and Sassoon 1998). Also in agreement with the present findings, *Wnt7a* null mice are refractory to estrogen-stimulated uterine weight gain (Carta and Sassoon 2004). In these mice, cell proliferation is intact, but cell death is much more pronounced; a similar mechanism could explain the dampened hormone-induced uterine weight gain in GEN-exposed mice. Taken together, these findings suggest that neonatal exposure to GEN or other estrogens down-regulate *Wnt7a* and its downstream targets, *Hoxa10*, *Hoxa11*, *Msx1*, and *Msx2* (Dunlap et al. 2011; Huang et al. 2005; Miller and Sassoon 1998), suggesting that *Wnt7a* is a key mediator of estrogen-induced uterine posteriorization and improper uterine responses and function later in life.

Uterine posteriorization is strongly associated with implantation failure in numerous mouse models, including gene deletions of *Msx1/2*, *Ctnnb1*, *Gata2, Smad1/5/4*, *Wnt4*, and *Sox17* (Franco et al. 2011; Jeong et al. 2009; Nallasamy et al. 2012; Rodriguez et al. 2016; Rubel et al. 2016; X Wang et al. 2018). The *Wnt4* and *Sox17* deletion models exhibited reduced gland formation and function, but LIF does not rescue implantation in either model (Franco et al. 2011; X Wang et al. 2018). These data suggest that posteriorization alone can also cause implantation failure. Coordinate with these findings, the *Foxa2* uterine overexpression mouse model has reduced gland numbers and posteriorization; the implantation failure is similarly not rescued by LIF (P Wang et al. 2018). Mice conditionally lacking *Msx1* and *Msx2* in the uterus have gene expression patterns typical of posteriorization, including increases in genes expressed in keratinized epidermis and ECM (Sun et al. 2016). Implantation failure in this model appears to result from a complete lack of embryo attachment to the endometrial epithelium; rescue by LIF was not attempted in this study (Nallasamy et al. 2012). In the present study, neonatal GEN exposure posteriorizes the female reproductive tract by reducing expression of *Wnt7a*, *Wnt4*, and multiple additional genes required for proper patterning. LIF's inability to rescue implantation in this model led us to conclude that uterine posteriorization contributes to the GEN-induced implantation failure phenotype.

Developmental exposure to other estrogenic chemicals such as DES and bisphenol A (BPA) results in alterations in uterine differentiation genes as well as posteriorization phenotypes, suggesting GEN is not unique and that its estrogenic properties underlie its mechanism of action (Hayashi et al. 2011; Smith and Taylor 2007; Yoshida et al. 1999). In fact, mice lacking estrogen receptor-alpha (*Esr1*) are refractory to DES-induced abnormalities (Couse et al. 2001). Several studies suggest that DES and other endocrine disrupting chemicals such as BPA alter the epigenetic landscape of the differentiating reproductive tract as a mechanism underlying phenotypic changes (Bromer et al. 2010; Jefferson et al. 2018; Li et al. 2018). Epigenetic changes include excessive accumulation of histone H3K27ac at enhancers occupied by ESR1 as well as DNA methylation changes. All of these studies show the importance of *Esr1* in mediating these effects, suggesting that any chemical with estrogenic activity could impact the developing reproductive system. Further research into the epigenetic signatures of estrogenic chemical exposures during critical periods of differentiation will expand our understanding of the mechanisms underlying the permanent nature of these changes.

Similar to rodents and sheep, proper human endometrial gland function appears to be required for implantation and maintenance of pregnancy throughout the first trimester (Burton et al. 2007; Dimitriadis et al. 2006; Spencer 2014). In humans, endometrial gland formation is initiated in the fetal period, but differentiation continues postnatally and is not complete until puberty (Gray et al. 2001; Valdes-Dapena 1973). This timeline of endometrial development and differentiation overlaps with the period in which infants might consume soy-based formulas. This sequence of events highlights the importance of recognizing sensitive windows of development, that is, developmental periods when exposures cause phenotypic effects, even when the same exposure has no effects at other times in life. Female infants consuming soy-based formulas exhibit changes in the vaginal epithelium and uterine volume characteristic of exposure to exogenous estrogens (Adgent et al. 2018). Epidemiological studies have shown increased fibroid size and longer, more painful menstrual cycles in women who consumed soy-based formulas as infants compared with cow milk formulas (D'Aloisio et al. 2012; Upson et al. 2016, 2019). However, fertility has not been assessed in this population of women. The data presented herein warrant further investigation of soy-based formula consumption in female infants and the long-term impact on reproductive function.

Acknowledgments

The authors thank the National Institutes of Health/National Institute of Environmental Sciences (NIH/NIEHS) Histology,

Immunohistochemistry, Imaging, and Molecular Genomics Cores and Comparative Medicine Branch for expert technical assistance with the project. We also thank F. DeMayo and S. Hewitt for critical review of this manuscript. This research was supported by the Intramural Research Program of the NIH/NEIHS (grant 1ZIAES102405 to C.J.W.).

References

Adgent MA, Umbach DM, Zemel BS, Kelly A, Schall JI, Ford EG, et al. 2018. A longitudinal study of estrogen-responsive tissues and hormone concentrations in infants fed soy formula. J Clin Endocrinol Metab 103(5):1899–1909, PMID: 29506126, https://doi.org/10.1210/jc.2017-02249.

Adlercreutz H, Mazur W. 1997. Phyto-oestrogens and Western diseases. Ann Med 29(2):95–120, PMID: 9187225, https://doi.org/10.3109/07853899709113696.

Arora R, Fries A, Oelerich K, Marchuk K, Sabeur K, Giudice LC, et al. 2016. Insights from imaging the implanting embryo and the uterine environment in three dimensions. Development 143(24):4749–4754, PMID: 27836961, https://doi.org/10.1242/dev.144386.

Benson GV, Lim H, Paria BC, Satokata I, Dey SK, Maas RL. 1996. Mechanisms of reduced fertility in Hoxa-10 mutant mice: uterine homeosis and loss of maternal Hoxa-10 expression. Development 122(9):2687–2696, PMID: 8787743.

Bromer JG, Zhou Y, Taylor MB, Doherty L, Taylor HS. 2010. Bisphenol-A exposure *in utero* leads to epigenetic alterations in the developmental programming of uterine estrogen response. FASEB J 24(7):2273–2280, PMID: 20181937, https://doi.org/10.1096/fj.09-140533.

Burton GJ, Jauniaux E, Charnock-Jones DS. 2007. Human early placental development: potential roles of the endometrial glands. Placenta 28(suppl A):S64–S69, PMID: 17349689, https://doi.org/10.1016/j.placenta.2007.01.007.

Cao Y, Calafat AM, Doerge DR, Umbach DM, Bernbaum JC, Twaddle NC, et al. 2009. Isoflavones in urine, saliva, and blood of infants: data from a pilot study on the estrogenic activity of soy formula. J Expo Sci Environ Epidemiol 19(2):223–234, PMID: 18665197, https://doi.org/10.1038/jes.2008.44.

Carson FL, Hladik C. 2009. *Histotechnology. A Self-Instructional Text*. Chicago, IL: American Society for Clinical Pathology.

Carta L, Sassoon D. 2004. *Wnt7a* is a suppressor of cell death in the female reproductive tract and is required for postnatal and estrogen-mediated growth. Biol Reprod 71(2):444–454, PMID: 15070830, https://doi.org/10.1095/biolreprod.103.026534.

Cooke PS, Ekman GC, Kaur J, Davila J, Bagchi IC, Clark SG, et al. 2012. Brief exposure to progesterone during a critical neonatal window prevents uterine gland formation in mice. Biol Reprod 86(3):63, PMID: 22133692, https://doi.org/10.1095/biolreprod.111.097188.

Cooke PS, Spencer TE, Bartol FF, Hayashi K. 2013. Uterine glands: development, function and experimental model systems. Mol Hum Reprod 19(9):547–558, PMID: 23619340, https://doi.org/10.1093/molehr/gat031.

Couse JF, Dixon D, Yates M, Moore AB, Ma L, Maas R, et al. 2001. Estrogen receptor-α knockout mice exhibit resistance to the developmental effects of neonatal diethylstilbestrol exposure on the female reproductive tract. Dev Biol 238(2):224–238, PMID: 11784006, https://doi.org/10.1006/dbio.2001.0413.

D'Aloisio AA, Baird DD, DeRoo LA, Sandler DP. 2012. Early-life exposures and early-onset uterine leiomyomata in black women in the Sister Study. Environ Health Perspect 120(3):406–412, PMID: 22049383, https://doi.org/10.1289/ehp.1103620.

Dimitriadis E, Stoikos C, Stafford-Bell M, Clark I, Paiva P, Kovacs G, et al. 2006. Interleukin-11, IL-11 receptorα and leukemia inhibitory factor are dysregulated in endometrium of infertile women with endometriosis during the implantation window. J Reprod Immunol 69(1):53–64, PMID: 16310857, https://doi.org/10.1016/j.jri.2005.07.004.

Doerge DR, Twaddle NC, Padilla Banks E, Jefferson WN, Newbold RR. 2002. Pharmacokinetic analysis in serum of genistein administered subcutaneously to neonatal mice. Cancer Lett 184(1):21–27, PMID: 12104044, https://doi.org/10.1016/S0304-3835(02)00200-8.

Du H, Taylor HS. 2015. The role of *Hox* genes in female reproductive tract development, adult function, and fertility. Cold Spring Harb Perspect Med 6(1):a023002, PMID: 26552702, https://doi.org/10.1101/cshperspect.a023002.

Dunlap KA, Filant J, Hayashi K, Rucker EB III, Song G, Deng JM, et al. 2011. Postnatal deletion of *Wnt7a* inhibits uterine gland morphogenesis and compromises adult fertility in mice. Biol Reprod 85(2):386–396, PMID: 21508348, https://doi.org/10.1095/biolreprod.111.091769.

Filant J, Lydon JP, Spencer TE. 2014. Integrated chromatin immunoprecipitation sequencing and microarray analysis identifies FOXA2 target genes in the glands of the mouse uterus. FASEB J 28(1):230–243, PMID: 24025729, https://doi.org/10.1096/fj.13-237446.

Filant J, Zhou H, Spencer TE. 2012. Progesterone inhibits uterine gland development in the neonatal mouse uterus. Biol Reprod 86(5):146, 1–9, PMID: 22238285, https://doi.org/10.1095/biolreprod.111.097089.

Franco HL, Dai D, Lee KY, Rubel CA, Roop D, Boerboom D, et al. 2011. WNT4 is a key regulator of normal postnatal uterine development and progesterone signaling during embryo implantation and decidualization in the mouse. FASEB J 25(4):1176–1187, PMID: 21163860, https://doi.org/10.1096/fj.10-175349.

Gray CA, Bartol FF, Tarleton BJ, Wiley AA, Johnson GA, Bazer FW, et al. 2001. Developmental biology of uterine glands. Biol Reprod 65(5):1311–1323, PMID: 11673245, https://doi.org/10.1095/biolreprod65.5.1311.

Gray CA, Bartol FF, Taylor KM, Wiley AA, Ramsey WS, Ott TL, et al. 2000. Ovine uterine gland knock-out model: effects of gland ablation on the estrous cycle. Biol Reprod 62(2):448–456, PMID: 10642586, https://doi.org/10.1095/biolreprod62.2.448.

Guimarães-Young A, Neff T, Dupuy AJ, Goodheart MJ. 2016. Conditional deletion of *Sox17* reveals complex effects on uterine adenogenesis and function. Dev Biol 414(2):219–227, PMID: 27102016, https://doi.org/10.1016/j.ydbio.2016.04.010.

Hayashi K, Erikson DW, Tilford SA, Bany BM, Maclean JA II, Rucker EB III, et al. 2009. *Wnt* genes in the mouse uterus: potential regulation of implantation. Biol Reprod 80(5):989–1000, PMID: 19164167, https://doi.org/10.1095/biolreprod.108.075416.

Hayashi K, Yoshioka S, Reardon SN, Rucker EB III, Spencer TE, DeMayo FJ, et al. 2011. WNTs in the neonatal mouse uterus: potential regulation of endometrial gland development. Biol Reprod 84(2):308–319, PMID: 20962251, https://doi.org/10.1095/biolreprod.110.088161.

Hewitt SC, Winuthayanon W, Pockette B, Kerns RT, Foley JF, Flagler N, et al. 2015. Development of phenotypic and transcriptional biomarkers to evaluate relative activity of potentially estrogenic chemicals in ovariectomized mice. Environ Health Perspect 123(4):344–352, PMID: 25575267, https://doi.org/10.1289/ehp.1307935.

Huang W-W, Yin Y, Bi Q, Chiang T-C, Garner N, Vuoristo J, et al. 2005. Developmental diethylstilbestrol exposure alters genetic pathways of uterine cytodifferentiation. Mol Endocrinol 19(3):669–682, PMID: 15591538, https://doi.org/10.1210/me.2004-0155.

Jefferson WN, Kinyamu HK, Wang T, Miranda AX, Padilla-Banks E, Suen AA, et al. 2018. Widespread enhancer activation via ERα mediates estrogen response in vivo during uterine development. Nucleic Acids Res 46(11):5487–5503, PMID: 29648668, https://doi.org/10.1093/nar/gky260.

Jefferson WN, Padilla-Banks E, Clark G, Newbold RR. 2002. Assessing estrogenic activity of phytochemicals using transcriptional activation and immature mouse uterotrophic responses. J Chromatogr B Analyt Technol Biomed Life Sci 777(1–2):179–189, PMID: 12270211, https://doi.org/10.1016/S1570-0232(02)00493-2.

Jefferson WN, Padilla-Banks E, Goulding EH, Lao S-P, Newbold RR, Williams CJ. 2009. Neonatal exposure to genistein disrupts ability of female mouse reproductive tract to support preimplantation embryo development and implantation. Biol Reprod 80(3):425–431, PMID: 19005167, https://doi.org/10.1095/biolreprod.108.073171.

Jefferson WN, Padilla-Banks E, Newbold RR. 2005. Adverse effects on female development and reproduction in CD-1 mice following neonatal exposure to the phytoestrogen genistein at environmentally relevant doses. Biol Reprod 73(4):798–806, PMID: 15930323, https://doi.org/10.1095/biolreprod.105.041277.

Jefferson WN, Padilla-Banks E, Phelps JY, Gerrish KE, Williams CJ. 2011. Permanent oviduct posteriorization after neonatal exposure to the phytoestrogen genistein. Environ Health Perspect 119(11):1575–1582, PMID: 21810550, https://doi.org/10.1289/ehp.1104018.

Jeong J-W, Kwak I, Lee KY, Kim TH, Large MJ, Stewart CL, et al. 2010. *Foxa2* is essential for mouse endometrial gland development and fertility. Biol Reprod 83(3):396–403, PMID: 20484741, https://doi.org/10.1095/biolreprod.109.083154.

Jeong J-W, Lee HS, Franco HL, Broaddus RR, Taketo MM, Tsai SY, et al. 2009. β-catenin mediates glandular formation and dysregulation of β-catenin induces hyperplasia formation in the murine uterus. Oncogene 28(1):31–40, PMID: 18806829, https://doi.org/10.1038/onc.2008.363.

Kelleher AM, Milano-Foster J, Behura SK, Spencer TE. 2018. Uterine glands coordinate on-time embryo implantation and impact endometrial decidualization for pregnancy success. Nat Commun 9(1):2435, PMID: 29934619, https://doi.org/10.1038/s41467-018-04848-8.

Kelleher AM, Peng W, Pru JK, Pru CA, DeMayo FJ, Spencer TE. 2017. Forkhead box a2 (FOXA2) is essential for uterine function and fertility. Proc Natl Acad Sci USA 114(6):E1018–E1026, PMID: 28049832, https://doi.org/10.1073/pnas.1618433114.

Koressaar T, Remm M. 2007. Enhancements and modifications of primer design program Primer3. Bioinformatics 23(10):1289–1291, PMID: 17379693, https://doi.org/10.1093/bioinformatics/btm091.

Kupershmidt I, Su QJ, Grewal A, Sundaresh S, Halperin I, Flynn J, et al. 2010. Ontology-based meta-analysis of global collections of high-throughput public data. PLoS One 5(9):e13066, PMID: 20927376, https://doi.org/10.1371/journal.pone.0013066.

Kurita T, Cooke PS, Cunha GR. 2001. Epithelial-stromal tissue interaction in paramesonephric (Müllerian) epithelial differentiation. Dev Biol 240(1):194–211, PMID: 11784056, https://doi.org/10.1006/dbio.2001.0458.

Kurzer MS, Xu X. 1997. Dietary phytoestrogens. Annu Rev Nutr 17:353–381, PMID: 9240932, https://doi.org/10.1146/annurev.nutr.17.1.353.

Laguë M-N, Detmar J, Paquet M, Boyer A, Richards JS, Adamson SL, et al. 2010. Decidual PTEN expression is required for trophoblast invasion in the mouse. Am J Physiol Endocrinol Metab 299(6):E936–E946, PMID: 20858757, https://doi.org/10.1152/ajpendo.00255.2010.

Large MJ, Wetendorf M, Lanz RB, Hartig SM, Creighton CJ, Mancini MA, et al. 2014. The epidermal growth factor receptor critically regulates endometrial function during early pregnancy. PLoS Genet 10(6):e1004451, PMID: 24945252, https://doi.org/10.1371/journal.pgen.1004451.

Lee KY, Jeong J-W, Tsai SY, Lydon JP, DeMayo FJ. 2007. Mouse models of implantation. Trends Endocrinol Metab 18(6):234–239, PMID: 17588769, https://doi.org/10.1016/j.tem.2007.06.002.

Li Y, Hamilton KJ, Wang T, Coons LA, Jefferson WN, Li R, et al. 2018. DNA methylation and transcriptome aberrations mediated by ERα in mouse seminal vesicles following developmental DES exposure. Proc Natl Acad Sci USA 115(18): E4189–E4198, PMID: 29666266, https://doi.org/10.1073/pnas.1719010115.

Messina M, Nagata C, Wu AH. 2006. Estimated Asian adult soy protein and isoflavone intakes. Nutr Cancer 55(1):1–12, PMID: 16965235, https://doi.org/10.1207/s15327914nc5501_1.

Miller C, Sassoon DA. 1998. Wnt-7a maintains appropriate uterine patterning during the development of the mouse female reproductive tract. Development 125(16):3201–3211, PMID: 9671592.

Mucenski ML, Mahoney R, Adam M, Potter AS, Potter SS. 2019. Single cell RNA-seq study of wild type and Hox9,10,11 mutant developing uterus. Sci Rep 9(1):4557, PMID: 30872674, https://doi.org/10.1038/s41598-019-40923-w.

Munro BH. 1971. Manual of histologic staining methods of the Armed Forces Institute of Pathology. Pathology 3(3):249, https://doi.org/10.1016/S0031-3025(16)39410-7.

Nallasamy S, Li Q, Bagchi MK, Bagchi IC. 2012. *Msx* homeobox genes critically regulate embryo implantation by controlling paracrine signaling between uterine stroma and epithelium. PLoS Genet 8(2):e1002500, PMID: 22383889, https://doi.org/10.1371/journal.pgen.1002500.

Namiki T, Ito J, Kashiwazaki N. 2018. Molecular mechanisms of embryonic implantation in mammals: lessons from the gene manipulation of mice. Reprod Med Biol 17(4):331–342, PMID: 30377389, https://doi.org/10.1002/rmb2.12103.

Newbold RR, Padilla Banks E, Bullock B, Jefferson WN. 2001. Uterine adenocarcinoma in mice treated neonatally with genistein. Cancer Res 61(11):4325–4328, PMID: 11389053.

Paria BC, Tan J, Lubahn DB, Dey SK, Das SK. 1999. Uterine decidual response occurs in estrogen receptor-α-deficient mice. Endocrinology 140(6):2704–2710, PMID: 10342861, https://doi.org/10.1210/endo.140.6.6825.

Raines AM, Adam M, Magella B, Meyer SE, Grimes HL, Dey SK, et al. 2013. Recombineering-based dissection of flanking and paralogous *Hox* gene functions in mouse reproductive tracts. Development 140(14):2942–2952, PMID: 23760953, https://doi.org/10.1242/dev.092569.

Reed CE, Fenton SE. 2013. Exposure to diethylstilbestrol during sensitive life stages: a legacy of heritable health effects. Birth Defects Res C Embryo Today 99(2):134–146, PMID: 23897597, https://doi.org/10.1002/bdrc.21035.

Rodriguez A, Tripurani SK, Burton JC, Clementi C, Larina I, Pangas SA. 2016. SMAD signaling is required for structural integrity of the female reproductive tract and uterine function during early pregnancy in mice. Biol Reprod 95(2):44, PMID: 27335065, https://doi.org/10.1095/biolreprod.116.139477.

Rubel CA, Wu SP, Lin L, Wang T, Lanz RB, Li X, et al. 2016. A *Gata2*-dependent transcription network regulates uterine progesterone responsiveness and endometrial function. Cell Rep 17(5):1414–1425, PMID: 27783953, https://doi.org/10.1016/j.celrep.2016.09.093.

Salleh N, Giribabu N. 2014. Leukemia inhibitory factor: roles in embryo implantation and in nonhormonal contraception. ScientificWorldJournal 2014:201514, PMID: 25152902, https://doi.org/10.1155/2014/201514.

Setchell KDR, Zimmer-Nechemias L, Cai J, Heubi JE. 1997. Exposure of infants to phyto-oestrogens from soy-based infant formula. Lancet 350(9070):23–27, PMID: 9217716, https://doi.org/10.1016/S0140-6736(96)09480-9.

Smith CC, Taylor HS. 2007. Xenoestrogen exposure imprints expression of genes (Hoxa10) required for normal uterine development. FASEB J 21(1):239–246, PMID: 17093138, https://doi.org/10.1096/fj.06-6635com.

Soyal SM, Mukherjee A, Lee KYS, Li J, Li H, DeMayo FJ, et al. 2005. Cre-mediated recombination in cell lineages that express the progesterone receptor. Genesis 41(2):58–66, PMID: 15682389, https://doi.org/10.1002/gene.20098.

Spencer TE. 2014. Biological roles of uterine glands in pregnancy. Semin Reprod Med 32(5):346–357, PMID: 24959816, https://doi.org/10.1055/s-0034-1376354.

Stewart CL, Kaspar P, Brunet LJ, Bhatt H, Gadi I, Köntgen F, et al. 1992. Blastocyst implantation depends on maternal expression of leukaemia inhibitory factor. Nature 359(6390):76–79, PMID: 1522892, https://doi.org/10.1038/359076a0.

Suen AA, Jefferson WN, Williams CJ, Wood CE. 2018. Differentiation patterns of uterine carcinomas and precursor lesions induced by neonatal estrogen exposure in mice. Toxicol Pathol 46(5):574–596, PMID: 29895210, https://doi.org/10.1177/0192623318779326.

Suen AA, Jefferson WN, Wood CE, Padilla-Banks E, Bae-Jump VLL, Williams CJ. 2016. SIX1 oncoprotein as a biomarker in a model of hormonal carcinogenesis and in human endometrial cancer. Mol Cancer Res 14(9):849–858, PMID: 27259717, https://doi.org/10.1158/1541-7786.MCR-16-0084.

Sun X, Park CB, Deng W, Potter SS, Dey SK. 2016. Uterine inactivation of muscle segment homeobox (*Msx*) genes alters epithelial cell junction proteins during embryo implantation. FASEB J 30(4):1425–1435, PMID: 26667042, https://doi.org/10.1096/fj.15-282798.

Taylor HS, Vanden Heuvel GB, Igarashi P. 1997. A conserved *Hox* axis in the mouse and human female reproductive system: late establishment and persistent adult expression of the *Hoxa* cluster genes. Biol Reprod 57:1336–1345, PMID: 9408238, https://doi.org/10.1095/biolreprod57.6.1338.

Upson K, Adgent MA, Wegienka G, Baird DD. 2019. Soy-based infant formula feeding and menstrual pain in a cohort of women aged 23–35 years. Hum Reprod 34(1):148–154, PMID: 30412246, https://doi.org/10.1093/humrep/dey303.

Upson K, Harmon QE, Baird DD. 2016. Soy-based infant formula feeding and ultrasound-detected uterine fibroids among young African-American women with no prior clinical diagnosis of fibroids. Environ Health Perspect 124(6):769–775, PMID: 26565393, https://doi.org/10.1289/ehp.1510082.

Valdes-Dapena MA. 1973. The development of the uterus in late fetal life, infancy, and childhood. In: *The Uterus*. Norris HJ, Hertig AT, Abell MR, eds. Baltimore, MD: Williams and Wilkins, 40–67.

Verkasalo PK, Appleby PN, Allen NE, Davey G, Adlercreutz H, Key TJ. 2001. Soya intake and plasma concentrations of daidzein and genistein: validity of dietary assessment among eighty British women (Oxford arm of the European Prospective Investigation into Cancer and Nutrition). Br J Nutr 86(3):415–421, PMID: 11570994, https://doi.org/10.1079/bjn2001424.

Wang P, Wu S-P, Brooks KE, Kelleher AM, Milano-Foster JJ, DeMayo FJ, et al. 2018. Generation of mouse for conditional expression of forkhead box A2. Endocrinology 159(4):1897–1909, PMID: 29546371, https://doi.org/10.1210/en.2018-00158.

Wang X, Li X, Wang T, Wu S-P, Jeong J-W, Kim TH, et al. 2018. SOX17 regulates uterine epithelial–stromal cross-talk acting via a distal enhancer upstream of *Ihh*. Nat Commun 9(1):4421, PMID: 30356064, https://doi.org/10.1038/s41467-018-06652-w.

Wu AH, Yu MC, Tseng C-C, Twaddle NC, Doerge DR. 2004. Plasma isoflavone levels versus self-reported soy isoflavone levels in Asian-American women in Los Angeles County. Carcinogenesis 25(1):77–81, PMID: 14555615, https://doi.org/10.1093/carcin/bgg189.

Yoshida A, Newbold RR, Dixon D. 1999. Effects of neonatal diethylstilbestrol (DES) exposure on morphology and growth patterns of endometrial epithelial cells in CD-1 mice. Toxicol Pathol 27(3):325–333, PMID: 10356709, https://doi.org/10.1177/019262339902700308.